NATIONAL UNIVERSITY OF SCIENCE AND TECHNOLOGY POLITEHNICA BUCHAREST

Doctoral School of Mechanical Engineering and Mechatronics

DOCTORAL THESIS

- SUMMARY -

NUMERICAL AND EXPERIMENTAL ANALYSIS OF STATIC OR DYNAMIC COMPRESSION BEHAVIOR OF POROUS MATERIALS IMBIBED WITH LIQUIDS

Doctoral student: *Eng.* ***Georgian-Cristian LUPU***

PhD supervisor: *Prof. Dr. Eng.* ***Traian CICONE***

BUCHAREST
October 2023

CONTENT

FOREWORD

The present doctoral thesis represents the synthesis of the scientific research activities that I performed between October 2018 and September 2023. The doctoral studies were carried out in the Dept. of Machine Elements and Tribology of the Faculty of Mechanical and Mechatronic Engineering from (the former) Politehnica University of Bucharest. During this period, I had the chance to participate in two research internships as part of the TriboLub team (Mécanique des Interfaces Lubrifiées) in the Angoulême location, part of Dept. Génie Mécanique et Systèmes Complexes, Institut PPRIME (Université de Poitiers). The internships were financed through the Erasmus+ program and their duration were 4 and 5 months respectively (March-July 2021 and January-May 2023). Also, during my last year of study, I benefited from financial support through the project "Preparation of doctoral students and researchers postdoctoral in order to acquire applied research skills – SMART", MySMIS code 153734, co-financed by the European Social Fund (ESF), through "Human Capital Operational Program (POCU)" 2014-2020.

I am now at a point where I am completing an important and challenging stage of my professional training and I notice, first of all, the progress I have made as a social being. Because doctoral studies are not only about theories, conclusions, or perspectives. Above all, this period is about the people who stood by me and without whom I could not have achieved anything. My thoughts and all the gratitude I can express in words are now directed towards them.

I would like to start by thanking to my PhD supervisor, Prof. Traian CICONE, first, for agreeing eight years ago to guide me towards the completion of my master's degree. Second, I thank him for giving me the honor of being his first student to complete the doctorate. I wish one day to repay the trust and energy he invested in me! Collaborating with the professor gave me the privilege of having by my side a man of great professional value involved both scientifically and humanly. Through passion and tenacity, he inspired me to continually exceed myself. I thank him for sharing his vast knowledge of tribology or numerical methods, amongst numerous others. I thank him for the moral support and for the mastery with which he always managed to make me reconsider, especially at times when I wanted to give up.

I want to thank Prof. Aurelian FĂTU for honoring me by accepting to participate in the doctoral committee, for his analysis of the paper and his valuable comments. Participating in the research internships gave me the opportunity to collaborate with him. His elegant, persevering style and vast knowledge of numerical analysis, tribology among the many others, led me towards obtaining and deciphering huge parts from the complex results presented in the thesis. I am deeply grateful for his total involvement in the modeling of the compression behavior of the 3D spacer and of the fluid flow through the yarns. I have learned enormously from him and surely this moment would have been much further away in time if I had not had the chance to work with a consummate and passionate professional like him. I thank him for always taking care to make my stay more pleasant during the two internships. I especially appreciate the positive energy and sense of humor with which he often managed to get me through the disappointments specific to experimental trials.

I have special respect for Prof. Mircea D. PASCOVICI who agreed to analyze my doctoral thesis and to be part of the doctoral committee. It is a huge honor for me that, the mentor of my professor and of so many generations of doctoral students whom he led with professionalism, scientific and academic rigor in the field of tribology and XPHD lubrication, agreed to participate in the evaluation process of the results of my doctoral studies. I owe him immense gratitude for the constructive appreciations he gave me during my scientific reports, for the creative ideas he shared, but especially for the smiles and positive energy he gave me every time I had the opportunity of having a conversation with you.

I would like to thank Prof. Ilie MUSCĂ from "Ștefan cel Mare" University of Suceava for honoring me by accepting to be part of the doctoral committee, for his time given to reading and analyzing the paper as well as for the comments made. I also want to thank Prof. Radu CHIRIAC for chairing the committee.

I thank lect. Petrică TURTOI for the support and professionalism in the articles written together, for the interpretation of the experimental data obtained, but especially for the valuable comments and

observations received during my research reports, in his role as a member of the guidance committee. I am also deeply grateful to him for his kindness, generosity, and moral support throughout the entire period.

I would like to especially thank the members of the guidance committee, Prof. Adrian PREDESCU and lect. Nicolae STOICA, for their valuable advice and for the constructive criticism of the scientific reports, which thus increased the value of the works developed.

I thank the members of the PPRIME laboratory, especially to assoc. prof. Yann HENRY for his decisive contribution and involvement in the realization of the cyclic compression bench and not only, as well as to assoc. prof Mohamed JARRAY for the valuable advice and guidance during the numerical simulations carried out in Fluent. Thoughts of special gratitude also go to Baptiste COUDERC for the innovative spirit and technical knowledge that helped to modify the experimental bench. For this, I also want to thank Mr. technician Cédric DELIAS for the support offered in assembling the device. Last but not least, I would like to thank the PhD students from the PPRIME and XLIM laboratories, for the warmth with which they welcomed me, especially Maxime LANG, for the beautiful memories and funny moments.

I respectfully thank Mr. technician Mihai ROZOREA for his help provided during the entire period. He is a man and a specialist whom I admire a lot because he always puts himself, with passion and creativity, at the disposal of students, to make the ingenious devices needed in their research activities.

To my doctoral colleague, Alice MARINESCU, I am grateful for the help provided in carrying out the compression tests at constant speed and for her involvement in obtaining the computed micro-tomography of the 3D spacer. I thank her, particularly, for the moral support in the difficult moments, for the advice and considerate words sincerely offered during my second Erasmus internship, in which we had the chance to exchanging opinions, both on scientific and personal level.

I want to thank lect. Dragoș APOSTOL from the Dept. of Resistance of Materials for the support provided in obtaining the results at constant speed compression. I would also particularly like to thank doctoral student Cătălin ENESCU for the permeability measurements he made for the comparison with the numerical results. I thank Mr. Eduard MOSES for his valuable advice on using Ansys Fluent.

I sincerely thank Mr. Octavian NICA and Mr. Octavian URECHE from ICPEST for the help and technical support provided in the last year. I would also like to thank Mr. Florin PISICĂ and Mr. Florin SAMOILĂ from Top Metrology (Romania) whose generous contribution with a professional 3D scan made the obtained results more valuable.

I thank my colleagues and the management board at the Military Engineering and Technology Research Agency for their support and understanding throughout this time.

I would like to express my thoughts of gratitude to my parents, extended family and friends who understood my efforts during this time and who supported and encouraged me.

Last but not least, I would like to thank my fiancée BEATRICE, for her patience, understanding and unconditional support throughout the whole period, without which I could not have achieved anything!

At this moment I am experiencing conflicting emotions, being happy to complete a complicated period, but also sad because the last cycle of my student life is coming to an end. But "every new beginning comes from the end of another beginning" (Seneca). My entire academic training has been a tortuous path through complex and challenging notions, full of ups and downs but never too difficult because I have had consummate professionals and people of extraordinary quality by my side whom I wish to pass on once again, with esteem and great respect, a simple and sincere...

THANK YOU !

Keywords: soft-porous materials, 3D textiles, reticulated foams, Newtonian fluid, ex-poro-hydrodynamic lubrication, compressive squeeze, permeability-porosity, critical porosity, cyclic compression frequency, reabsorption, computed micro-tomography, periodic representative cell, nonlinear structural analysis, CFD analysis, Darcy flow, Darcy-Forchheimer flow

INTRODUCTION

At the origin of the activities carried out during my doctoral formation are the studies developed over the last 20 years in the Lubrication Laboratory (Department of Machine Elements and Tribology) from PUB, focused on the use of highly deformable porous layers, imbibed with liquids, as a reduction solution of impact effects.

The mechanism that produces this effect was named ex-poro-hydrodynamic lubrication (XPHD) by the one who initiated and led these studies, Prof. M. D. Pascovici. The mechanism is based on the resistance to flow through the porous structure, subjected to normal compression. Compression continuously changes the porosity and implicitly the permeability, which makes the resistance to the fluid flow increasing.

The same mechanism can have positive effects in the generation of hydrodynamic pressures even in the case of a sliding motion. Studies in this direction were started about 10 years ago by the Angoulême team of the Pprime Institute, led by Prof. Aurelian Fătu.

Hence the common interest of the two teams, that led to joint research activities on fluid flow through porous materials. The studies presented in this thesis took place in this framework, which included two internships of 4 months each at the Pprime Institute.

The approach to this subject involves multi-disciplinary studies on the morphology and compressibility of porous materials, on their permeability correlated with porosity, as well as studies of fluid rheology and modeling of flow through the porous structure under variable compression conditions.

The studies presented in this paper try to clarify some fundamental aspects of the flow of Newtonian fluids through the communicating pores of some soft, porous materials, subject to compression, to use them for impact attenuation, cushioning, or the generation of lift effect through translational motion.

These last observations revealed from the bibliographic study led to the objectives of the studies carried out within the doctoral program, namely:

- Determination, through numerical simulation, of the inertial effects influence (Darcy-Forchheimer flow) on the liquids squeezed through compressible porous media, which also lead to establishing the limits of the use of Darcy flow model (laminar flow).
- Emphasizing, experimentally, the effective limit porosity (critical porosity) from which the pores close and the flow through the porous layer is no longer possible.
- Experimental study on the damping and re-imbibement capacity of porous materials, soaked with liquids, subjected to cyclic compression.
- Complex numerical simulation of the structural evolution of three-dimensional textiles under compression.

- Complex numerical simulation (CFD) of fluid flow through the fibrous structure of three-dimensional textiles correlated with the structural configuration modified by compression.

The thesis is structured in five important chapters:

- *Chapter 1* presents the current state of research for the subject addressed, namely the characterization of the porous materials of interest, the modeling of flow through porous materials. An important part is dedicated to the description of three-dimensional textiles and the attempts to model their compression behavior.
- *Chapter 2* presents an analysis model of the flow of a Newtonian fluid through a porous layer, axially symmetric, under continuous compression, considering inertial effects (Darcy-Forchheimer flow). The chapter also includes an analysis of the influence of some parameters on the pressure distribution generated by compression.
- *Chapter 3* is dedicated to the analysis of the permeability limit of open-pore reticulated porous materials. An original experimental device, the methodology used and the results obtained are presented.
- *Chapter 4* includes an experimental analysis of the damping capacity of two porous materials of interest (reticulated structures and 3D textiles respectively) under cyclic compression conditions. The study highlights the reabsorbing capacity of the porous medium as a function of the frequency of compression and the level of compression.
- *Chapter 5,* the most extensive, includes a simulation of the compression behavior of a three-dimensional textile material (Spacer 3D) digitized following a complex processing of the images obtained by computerized micro-tomography and the comparison with my own experimental results. In the second part of the chapter, the flow of a Newtonian fluid is simulated, through the compressed structure at different levels, to determine the variation of permeability with porosity. The results are compared with experimental data from third-party sources.

The thesis ends with a chapter of conclusions, an enumeration of the main contributions, with an emphasis on the novelty elements, as well as with the marking of some directions of evolution in the knowledge of the studied processes.

CHAPTER 1
BIBLIOGRAPHIC STUDY

Starting from 1994, Prof. MD Pascovici (PUB) highlights the quality of easily deformable porous materials to generate lift effects, when imbibed with a fluid, and analyzes the connection between the flow of a fluid through the communicating pores and their accentuated deformation [72]. The process was named ex-poro-hydrodynamic lubrication[1](XPHD) [73].

Compared to the classic hydrodynamic regime, the load capacity is higher (for the same geometry, speed, and lubricant) [74]. The ability of imbibed porous materials to provide superior load capacity was independently analyzed and confirmed by the results of teams led by Prof. S. Weinbaum (City University, New York [28], [103]) and LJ Gibson (MIT [21]), thus giving it an international character.

As some experimental results have proven difficult to correlate theoretically, it is necessary to test the limits of the simplifying assumptions of XPHD lubrication to obtain a model with wide applicability.

1.1 PROPERTIES OF HIGHLY COMPRESSIBLE POROUS MEDIA

1.1.1 Porous medium definition

Some important definitions of the porous medium are presented ([6], [7], [8]) and also the way to approach the transport phenomena (at the micro and macro level) associated with the flow of fluids through the pores of the structure, pointing out the trends in the field and some critical aspects ([83], [89]).

1.1.2 Porosity

1.1.2.1 Definition. Classification

Porosity (ε), effective porosity (ε_{ef}) [88]and the inverse size of porosity (compactness) are defined. Some important aspects about the structure of porous media and the impact of different types of pores encountered on the process of flow through them are presented [85].

1.1.2.2 Methods determining porosity

Direct methods for determining porosity are briefly described.

1.1.2.2.1 Determining porosity by computer tomography

Several advantages of using micro-computed tomography for the study of porosity at different stages of material compression are presented ([49]), as well as for the reconstruction of the internal structure of some textile porous materials ([40]).

[1]The name was obtained by combining three terms necessary for the appearance of this mechanism: "ex-" (the expulsion/extraction of the fluid), "poro-" (through/from the pores of the porous structure) and "hydrodynamic" (through the development of forces generated by moving the fluid from the porous gap). [73]

1.1.2.2.2 Determination of porosity by the volumetric method

The method used to determine the effective initial porosity ($\varepsilon_{0_{ef}}$) of some materials of interest for XPHD lubrication is described. The results of some measurements done in previous studies and some observations on the accuracy of the method are presented ([92], [81]).

1.1.3 Permeability

Permeability (ϕ) is defined, its measurement units are presented and the method of calculating the intrinsic permeability of porous materials is described, from experimentally determined data and the Darcy flow model [17].

The different ways of determining permeability for woven or fiber materials are mentioned, depending on their isotropy ([32], [55]). Also, the difference between static and dynamic permeability is presented, which occurs at high flow rates due to the rapid deformation of the solid matrix or the appearance of a shock wave [101].

1.1.4 Correlation of permeability with porosity

1.1.4.1 Theoretical correlations

The limitations of different variants of capillary channel models, based on Hagen-Poiseuille theory, are pointed out, and two new geometrical properties (average specific surface area and tortuosity) proposed for their improvement in [88] are presented.

From capillary channel models derive theories using the hydraulic radius concept, from the observation that permeability is the size of an area. The Kozeny-Carman relationship ([48], [13]), used in the theoretical modeling of the Pascovici group is presented in the form [34]:

$$\phi = \frac{D\varepsilon^3}{(1-\varepsilon)^2} \tag{1.1}$$

In relationship (1.1), $D = d_f^2/16k$, d_f is the average diameter of the material fibers and k, an empirically determined factor (in the range of 5÷10) for correlating $\phi - \varepsilon$.

A final category of models is based on flow resistance theory, which considers pore walls as obstacles that oppose resistance to the linear fluid flow. They differentiate, depending on the geometric form, into theories with obstacles in the form of fibers [25] or in the form of spheres [12]and lead to good results for materials with high porosities.

1.1.4.2 Experimental correlations

Approaches from the literature regarding the determination of permeability and its correlation with the porosity for some technical porous materials are presented.

In studies ([103], [104], [64]) on very high porosity air-imbibed materials, the correlation of permeability with porosity, at low flow rates, is accurately described by Kozeny-Carman derived models, based on the variation of the factor $k$with porosity ([39], [91]).

It is recalled that the XPHD mechanism requires the determination of the permeability in the Darcy regime, for the identification of suitable materials and the completion of the Kozeny-Carman relation with the value of the parameter Din the relation (1.1). The homogeneity and

isotropy of the studied materials led to the construction or adaptation of experimental stands for permeability measurement.

For the materials analyzed in the Pascovici group, the Kozeny-Carman model ensures a good level of correlation of the experimental determinations. For medium porosity values, the observation is also valid when the fluid flow velocities no longer vary linearly with the imposed pressure gradient [93]. For low porosities, even under Darcy flow conditions, the Kozeny-Carman model underestimates the permeability by several orders of magnitude, requiring the identification of other correlation models or the use of empirical correction factor values k, different from the range indicated in the literature [26].

It is concluded that the Kozeny-Carman model does not always succeed in accurately correlating permeability with porosity and that most theoretical models present limitations, due to the particular conditions of the measurements. In the literature it is observed that different permeability values are obtained, even by an order of magnitude, between experiments carried out under the same conditions ([45], [59]). The complexity of the benches, the experimental costs and the practical limitations of flow measurement show the need for different approaches, through statistical or deterministic methods.

1.1.4.3 Critical porosity

A questionable aspect of the theoretical modeling of the correlation of permeability with porosity is presented, which assume that permeability becomes zero when porosity is also zero. This limitation has also been observed from studies analyzing the consolidation process of laminated composite materials, in which the emergence of a critical compactness from which fluid flow no longer occurs is highlighted ([37], [38], [32]).

The need to determine the non-zero (critical) porosity value is emphasized, especially for materials with high porosities, from which there are no more communicating (open) pores through which the fluid can flow.

1.2 THE EQUATIONS OF FLOW THROUGH POROUS MEDIA

The utility of the macroscopic approach to analyze flow through porous media is discussed and the concept of representative elementary volume (VER) is presented [68]. The essential condition for flow through porous media is emphasized (the existence of communicating pores along the medium) and the materials that have all the pores connected are introduced, which are also called reticulated porous materials ([18], [19], [20], [21]).

1.2.1 Darcy's Law

Darcy's law is presented, for a homogeneous and isotropic medium occupied by an incompressible fluid, when the influence of the gravitational force is neglected ([88], [68]):

$$grad\ P = -\frac{\eta}{\phi}\vec{u} \tag{1.2}$$

The applicability of the model, limited to media with low permeabilities and laminar flow with low velocities, is analyzed. Other objectionable aspects of the model are presented, such as not considering the influence of fluid friction around the walls or the inertial effects of the fluid that lead to a non-linear increase in the flow velocity.

1.2.2 Forchheimer correction

The most suitable modification of relation (1.2) to consider inertial effects ([46], [47]), known as Darcy-Forchheimer, is presented:

$$\nabla P = -\frac{\eta}{\phi}\vec{u} - \frac{C_f \rho}{\sqrt{\phi}}|\vec{u}|\vec{u} \tag{1.3}$$

The dimensionless parameter $C_f$is called the Forchheimer coefficient ([23], [29]). The term $C_f/\sqrt{\phi}$ represents the form drag term, derived from the drag theory ([4], [10]). Various attempts to define the parameter C_f are presented, either in the form of a universal constant (0.55) or in a variable form ([102], [9], [52], [68]).

A tendency to use the Reynolds number characteristic to flow through porous media (Re_p) is observed, to analyze deviations from the linearity of the Darcy model, and its formula is presented, when expressed as a function of permeability ([102], [50], [10]):

$$Re_\phi = \frac{\rho\sqrt{\phi}}{\eta}u \tag{1.4}$$

Re_p can also be defined by other characteristic dimensions of the porous medium, such as porosity or an average diameter of the matrix constituents, but there are some criticisms on the use of the average diameter, which would lead to overestimated values ([14], [71]).

An analysis of the upper limit of Darcy's law is performed, depending on the value of Re_p. The general consensus is that after $Re_p > 1$ the flow velocity no longer varies directly proportional to the pressure gradient ([31], [6], [90]), but the flow remains laminar [24]. After this value, a mixed regime appears in which viscous and inertial effects coexist, but the limit of the interval is still a subject to debate, the most common values being $Re_p = 1 \div 5$ ([99], [30]) or $Re_p = 1 \div 10$ ([6], [14], [24]).

It is concluded that these limits are specific to the analyzed porous media and should not be considered universally valid, as very different critical values of Re_p have been identified [100]. Regarding the Darcy-Forchheimer model, there are more and more opinions that assume that it is permanently present, the predominantly viscous or inertial effect evolving with increasing flow regime ([100], [70], [51]).

1.2.3 Studies on flow through materials subject to compression

The subject of flow through porous media is addressed in many studies, theoretical or experimental, and an exhaustive description of them would be impossible. However, only a few addresses the equations of the flow of a fluid through porous materials subjected to compression, when they deform significantly.

Some studies are presented in which porous material deformation and permeability analysis were addressed, but in them the solid matrix is rigid and does not recover after deformation ([4], [10], [50]).

Another approach found in the literature, inspired by the functioning of synovial joints, refers to the study of flow through porous materials when a layer of fluid, suspended above a

rigid porous material, is forced through the material by compression at constant speed ([66], [65], [67]). The problem of the flow through the porous material is solved by simultaneously coupling, at the fluid film - porous disc interface, the equations of the flow in the fluid film with those describing the flow in the porous medium.

1.3 XPHD LUBRICATION

1.3.1 Basic principles

Studies on the applicability of the XPHD mechanism in complex fields are presented, such as: viscosity pumps [72], axial bearings [73], erythrocyte lubrication in microcapillaries [75], natural or prosthetic human joints [76]. Studies are presented on the self-acting effect generated by XPHD lubrication, on multiple configurations, with compressive motion in the normal or tangential direction. Sphere/plane configurations [87], step [73]and plane-inclined surfaces [74] have been addressed for tangential motion. For normal motion, disc/plane configurations ([76], [95], [61], [15]), sphere/plane ([76], [42], [43], [77], [62]), cylinder/inner cylinder ([44]), perpendicular cylinder/cylinder ([82]) were analyzed. All studies use the simplifying assumptions stated in [73]:

- the fluid is Newtonian having laminar, isothermal, isoviscous flow
- compared to the flow resistance forces, the elastic forces are negligible
- across the thickness of the material, the fluid pressure is constant
- Darcy's law [17] characterizes the fluid flow
- the Kozeny-Carman law ([13], [48]) describes the permeability variation with porosity
- flow occurs in the plane perpendicular to the direction of compression
- during deformation, the solid fraction of the porous medium is preserved

1.3.2 XPHD model for constant velocity squeeze

1.3.2.1 Analytical model

The theoretical modeling of squeeze during normal compression has been oriented towards conformal contacts in disc/plane configuration [78], non-conforming contacts of sphere/plane type [76], [77] or a non-uniform configuration on a flat surface [80]. The study of the squeeze of a fluid from the porous material, positioned between surfaces in normal relative motion, is branched into the squeeze of the fluid at constant load (velocity or compressive force) and by impact.

Since the studies presented in this paper are focused on constant velocity squeeze, the theoretical model for the disc/plane configuration, developed by the Pascovici team, is presented. During normal compression, the geometry of the porous structure changes but the solid component of the porous layer remains constant throughout the thickness of the layer:

$$h(1-\varepsilon) = h_0(1-\varepsilon_0) = const. \tag{1.5}$$

The equation (1.5), known as the conservation of the solid fraction, allows to determine the minimum value of the thickness (h_{min}) at which zero porosity is reached by compressing the material. XPHD lubrication occurs only in the interval (h_0, h_{min}) [81], although the material can still be compressed after reaching zero porosity.

The configuration of the analytical model, in the case of constant velocity squeeze, on a disc/plane configuration, is shown in Figure 1.1. The modeling of constant velocity squeeze for parallel surfaces uses the flow conservation equation [81]. The volume of the solid matrix and the volume occupied by the fluid represent the total volume, and the flow rate displaced by the material is found in the flow rate flowing in the planar direction.

The analytical relation is obtained by considering a disc of porous material, of radius R, initial thickness h_0 and initial porosity ε_0, soaked with a Newtonian fluid of viscosity η. The material is subjected to compression with the velocity Wbetween a flat surface and a disc, considered rigid and impermeable. Since the disc is thin (relative to the radius), the thickness pressure is constant.

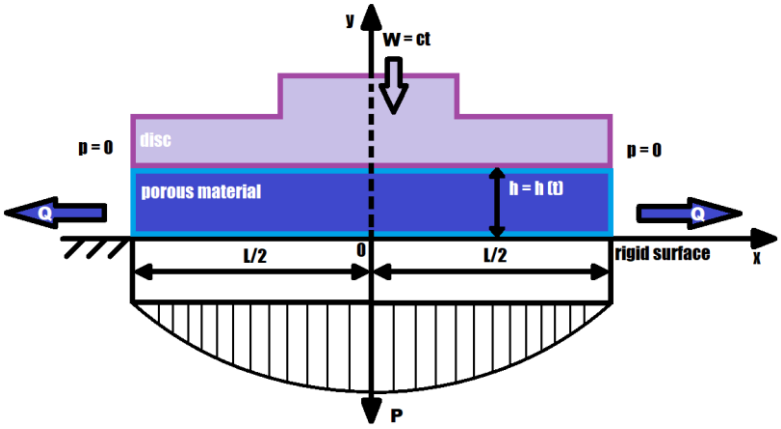

Figure 1.1 Disc/plane configuration

In the analytical (axial-symmetric) model, the pressure varies between zero (at $r = R$) and the maximum value (in the center, at $r = 0$). Considering that the permeability varies with the porosity according to the relation (1.1), the parabolic distribution of pressures on the disc surface is obtained. After integration (on the surface of the disc) the squeeze force for a certain level of compression is obtained:

$$F = 2\pi \int_0^R rP\,dr = \frac{\pi\eta W}{8D}\frac{(1-\varepsilon)^2}{\varepsilon^3 h}R^4 \tag{1.6}$$

Using the dimensionless expression of the thickness (from (1.5) $\bar{h} = h/h_0$) and the squeeze force written in the form $\bar{F} = FDh_0/\eta W R^4$ ([60]) results in the dimensionless force:

$$\bar{F} = \frac{\pi(1-\varepsilon_0)^2}{8\left(\bar{h}-1+\varepsilon_0\right)^3} \tag{1.7}$$

According to (1.7), the dimensionless force as a function of $\bar{h}$, depends only on ε_0.

1.3.2.2 Experimental results

In PUB, constant velocity compression tests were performed on the CETR-UMT2 Multi-Specimen Test System bench. Some observations of these tests are presented, the most important of which are:

- at small porosities (≈0.2) the fluid is completely displaced, but a small amount of liquid remains in the formed channels [79]

- upon decompression, normal force decreases values with increasing speed and the appearance of cavities, the liquid being absorbed inside them [41]
- high viscosity affects the beginning of the reabsorbing process, when more pronounced and longer depression (cavitation) phenomena occur [41]
- reducing the level of imbibition highlights the diminution of the XPHD effect [92]
- at the critical thickness from which the pores close, the material becomes like a solid body that initially deforms elastically [60]

A general conclusion is presented on the compression test at constant speed, which has the role of approximating a function of permeability variation in relation to different variables.

1.3.3 XPHD model for impact squeeze

The geometry for the case of squeeze by impact is the one presented in Figure 1.1. The displacement of the upper rigid disc occurs after the impact with a mass, M, falling with initial velocity W_0.In addition to the XPHD assumptions [73], it is presumed that the mass of the upper rigid disc is negligible and that, after the collision, the components in contact continue to move with the same initial velocity W_0 ([15]). The main assumption is considering the kinetic energy consumed by the upper disc equal to the mechanical work of the squeezed fluid, in the same unit of time, an approach used in [11] for the hydrodynamic impact squeeze process.

The solution is deduced using a quasi-static approach, starting from the relation (1.7). The force is assumed to be constant over an infinitesimal time interval, so that the variation of the force over the time of impact can be expressed using the theoretical model of constant velocity squeeze for each time step. Using the approach from [11], the velocity of the disc during the impact is obtained which, introduced into the expression of the dimensionless force (1.7), leads to the variation of the impact force for a given impulse in dimensionless form:

$$\bar{F}_i = \frac{\pi(1-\varepsilon_0)^2}{8\left(\bar{h}-1+\varepsilon_0\right)^3}\left\{1-\frac{\pi(1-\varepsilon_0)^2}{16\bar{M}}\left[\frac{1}{\left(\bar{h}-1+\varepsilon_0\right)^2}-\frac{1}{\varepsilon_0^2}\right]\right\} \tag{1.8}$$

In relation (1.8), $\bar{F}_i = F_i D h_0/\eta W_0 R^4$ and $\bar{M} = MDW_0/\eta R^4$ are dimensionless parameters. Maximum value of $\bar{F}_i$ in the relationship (1.8) is specific to ε_0 and increases with increasing impulse, being useful for characterizing the damping capacity of imbibed porous materials [15]. It is desired to obtain a maximum value as low as possible for better damping.

The damping capacity is evaluated with the dimensionless energy absorbed during compression, in which $\varepsilon_{0_{opt}}$, called the optimal value of the porosity that minimizes the maximum impact force, which depends only on the impulse $\bar{M}$. The higher the initial impulse, the less porosity is required to fully attenuate the impact through the squeeze effect [15].

A comparison of the analytical results with experiments is presented ([96],[15]). The tests, performed on spacer samples imbibed with glycerin and encapsulated in thin membranes, show that the impact forces are 60-70% lower than in dry state. The analytical results show a good predictability of the maximum impact forces, experimentally obtained. The compression level beyond which the XPHD model is no longer appliable needs to be determined. After this threshold level, the elastic forces should be considered as some fluid remains inside the pores, after the flow ceases.

1.4 EASILY DEFORMABLE POROUS MATERIALS WITH APPLICABILITY IN XPHD LUBRICATION

The conditions for a porous material to be useful in forming the XPHD lubrication mechanism are that it is easily compressible and has high porosity and communicating pores.

1.4.1 Woven and non-woven textiles

In general, the teams led by MD Pascovici were interested in synthetic materials characterized by macro-porosity, among cellular and fibrous materials. The most important aspects of textile materials, woven and non-woven, characterized in experimental activities, with the potential to be used in XPHD lubrication are presented ([41], [81], [92]).

In the experimental activities carried out in PUB, some reticulated foams with communicating pores and large porosities are highlighted, that led to promising results, both with Newtonian and non-Newtonian fluids [92]. Also, presenting a high potential to be used in impact damping applications [60], S3D type materials are analyzed in detail in this thesis.

1.4.2 Three-dimensional textiles

There is no standard definition for differentiating two-dimensional (2D) from three-dimensional (3D) textiles, although the structural variety or production process shows the need for one. There is a wide variety of 3D textile materials with different structures [86].

1.4.2.1 Definition of three-dimensional textiles

Distance fabrics with intertwined yarns are defined and the methods of obtaining them are presented. The material analyzed in this work is a warp-knitted spacer fabric ([54], [69], [105], [106]) shown in Figure 1.2 and referred to thereafter as *3D Spacer*. The material (annotated S3DU) is composed of two parallel faces knitted from multifilament fibers, interconnected by a middle layer formed by the vertical knitting of textile threads, generally monofilament, that ensure a certain distance between them.

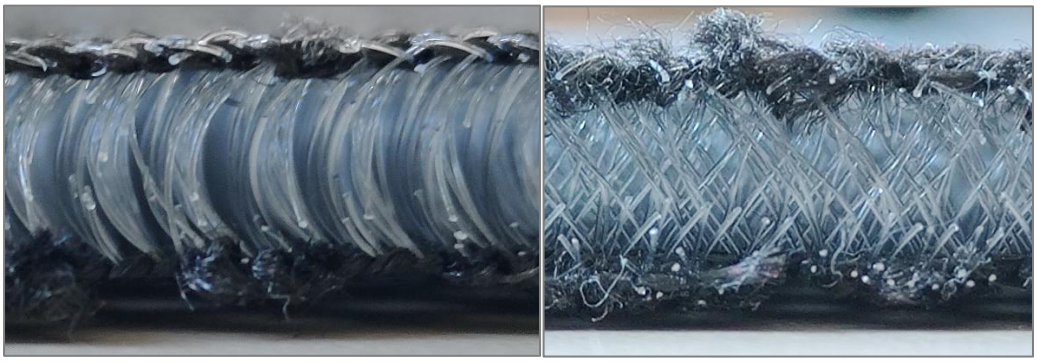

Figure 1.2 S3DU warp-knitted spacer fabric (side views)

1.4.2.2 Methods of analysis and characterization of three-dimensional textiles

The most important methods of analysis and characterization of S3DU materials are briefly presented. A study on the compression of an S3DU type material and the influence of some structural parameters on its nonlinear response is analyzed in ([40]). Specific compression curves

of dry S3DU specimens (Figure 1.3, left) present 4 distinct stages, delimited by the changes appearing in the slope of the curve ([40], [54]):

- stage I (initial): knitted between the multifilament yarns, the middle yarns slide easily in the thickness of the faces as they are not sufficiently constrained.
- stage II (linear elastic): the middle yarns bend slightly and fix better in the faces, increasing the stiffness of the material as the stress increases linearly with the strain.
- stage III (appearance of the plateau): the relatively constant stress enters a plateau as the middle yarns pass through several transformations (buckling, rotation, or shearing).
- stage IV (densification): when the stress starts to increase abruptly, the entire material begins to densify due to the "collapse" of the middle yarns and, towards the end, they come into contact with each other and with the faces of the material.

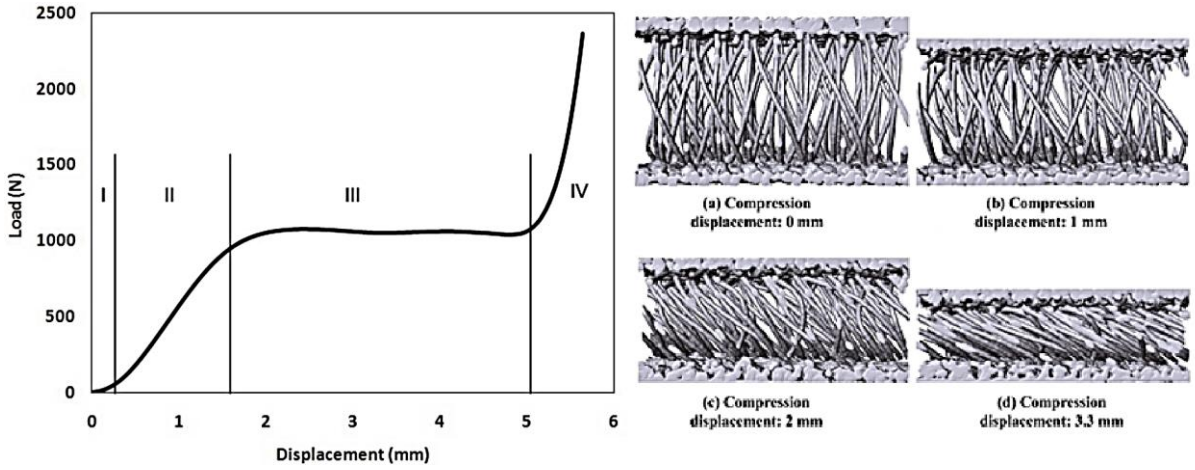

Figure 1.3 Compression stages of S3DU (left); Compressed material, scanned with µCT (right) [40]

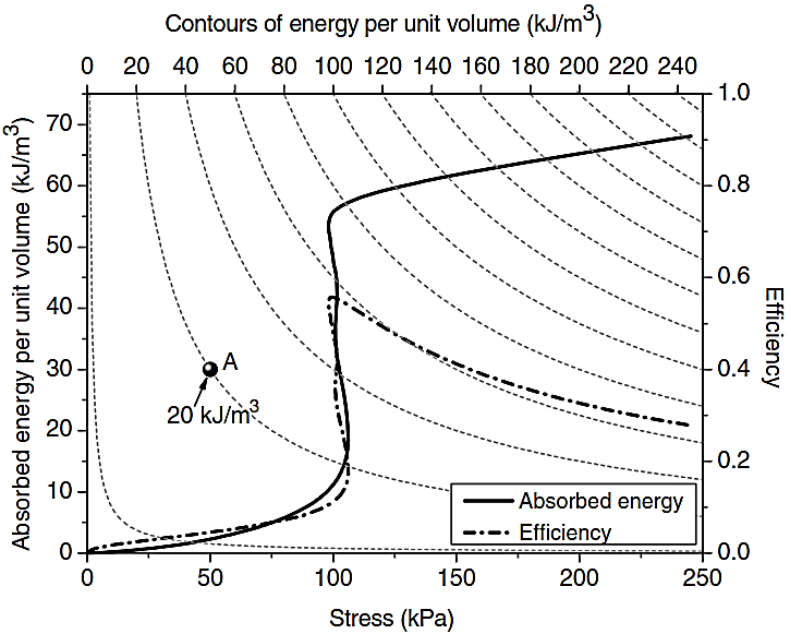

Figure 1.4 Absorbed energy and efficiency diagrams with stress for an S3DU material [54]

For the characterization of S3DU materials, when used in damping or impact protection applications, absorbed energy and efficiency diagrams are used (Figure 1.4) [54]. Developed from a model used for polyurethane foams [63], these diagrams result from the experimental curves obtained by compressing the material.

Constant stress under high compression (approx. 50% of original thickness) makes these materials suitable for damping applications. The area under the curve, covering the first three stages, represents the energy absorbed by the material, being relatively equivalent to the absorbed kinetic energy of a mass that could strike the material.

An approach used for the theoretical prediction of the macroscopic properties of an S3DU is presented, considering the microscopic properties of the fibers and the structure of the material [69]. The analyzed materials have the particularity that the distancing yarns are arranged symmetrically in the material structure, which allows a parametric modeling of the periodicity, the diameter of the fibers and the thickness of the material. The variation of permeability with material deformation is studied on a representative cell, which is repeated periodically in the material, and the results are extrapolated to the entire material.

1.4.3 Reticulated foams with communicating pores

1.4.3.1 Elements of theory of cellular porous materials

The aspects that led to the need to express permeability as a function of strain, especially in the case of cellular porous materials, are presented. These materials are predominantly rigid, but there are also easily deformable materials, called reticulated polyurethane foams, also studied by the research teams led by Prof. MD Pascovici ([81], [92]).

Structurally, these foams are made up of polyhedral cells. The properties of foams depend on [35]: cell shape (generally anisotropic), its size and type (closed or open/with communicating pores), relative density (calculated with respect to the solid material from which they are made), cell geometry (Voronoi structures, tetrakaidecahedron, etc.).

1.4.3.2 Compression of reticulated foams with communicating pores

The compression behavior of reticulated foams with communicating pores, in dry state, is described by three different regimes, which depend on the phenomena inside [35]:

- linear deformation stage: cell edges bend/curve.
- the plateau of nonlinear deformations: the solid structure deforms elastically/ buckles; for elastomers, the action is partially reversible.
- densification: the pores close and the edges of the cells touch.

The first stage is delimited by the Young's modulus characteristic of the porous structure E^*. It determines the linear variation of the strain, being dependent on the properties of the solid matrix, the relative density, and the geometrical conditions [35].

A second parameter of interest is the stress specific to the non-linear elastic deformations (σ_{el}^*), that appears at a deformation of approximately 5%. Densification strain δ_D depends on the density of the base material. In the densification stage, E^* is close to the solid from which the foam is made (E_S), without matching it, as porosity is impossible to be completely nullified.

1.4.3.3 Permeability of reticulated foams with communicating pores subjected to compression

The results of studies carried out on the variation of permeability with deformation are presented, from which the strong influence of the cell shape and the pore sizes through which

the fluid circulates is noted [33]. A mechanism found in the literature is described, based on with different material densities, which leads to an inhomogeneous deformation of foams due to cell buckling, an observation confirmed by experimental results ([36], [53], [20], [21]).

Finally, some results of some experimental studies, carried out with non-Newtonian fluids to characterize their behavior in impact applications, are presented. The difficulties to initially saturate the material as well as the application of this mechanism in reusable damping systems are highlighted ([22], [97], [98]).

1.5 CONCLUSIONS

Successful use in impact attenuation tests with liquid-saturated three-dimensional textiles and comparison with theoretically obtained numerical results showed significant differences, especially at higher impact velocities. They can have three important sources:

- At high impact velocities, inertial effects can be important and theoretical models based entirely on Darcy flow (laminar flow) become less accurate.
- At higher degrees of compression, the initially communicating pores begin to close and flow ceases before reaching zero porosity, the theoretical permeability limit used in most theoretical models.
- Questionable permeability values due to the lack of experiments carried out under similar experimental conditions.

The positive impact attenuation effects, emphasized theoretically and experimentally, have generated an interest to test the XPHD mechanism to cyclical motion, a situation in which the regeneration of the damping capacity through re-imbibing with liquid becomes essential.

CHAPTER 2
EVALUATION OF INERTIAL EFFECTS ON THE SQUEEZE OF NEWTONIAN FLUIDS FROM COMPRESSED SOFT, POROUS LAYERS. DISC/ PLANE CONFIGURATION

The simplifying assumptions (mentioned in chapter 1) were the basis of the analytical models for previously studied configurations and assume that the fluid flows through the porous medium according to the Darcy model. Since this model has been observed to have its applicability limited to low flow rates, the Dupuit-Forchheimer correction must be considered when increasing the flow regime. The configuration analyzed in this chapter is an easily deformable porous disc, imbibed with a Newtonian fluid and compressed between two plane-parallel surfaces. The assumption of the conservation of the solid component (1.5) during compression is used to determine the minimum thickness.

2.1 THE NUMERICAL MODEL

A numerical model was made for the studied configuration in which the porous material is subjected to a constant compression velocity, W. The plates are considered rigid, impermeable and remain parallel during compression, so the pressure distribution is symmetric

with respect to the OY axis. Thus, the numerical model (Figure 2.1) is considered axially symmetric. Since the layer of porous material is thin, during compression the pressure does not vary in the radial direction, so the fluid is flowing only in the axial plane.

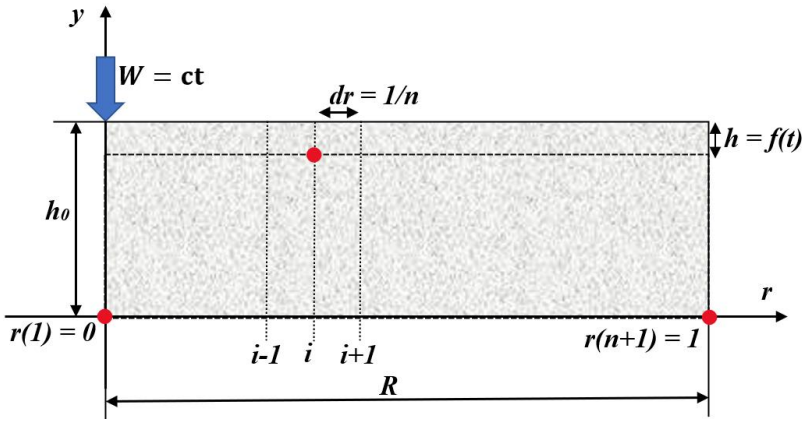

Figure 2.1 The disc/plane configuration of the numerical model

To obtain the mathematical model, one starts from the law of conservation of mass for an incompressible fluid, written in radial coordinates, for the case of axial-symmetric flow:

$$\frac{1}{r}\frac{\mathrm{d}}{\mathrm{d}r}(ru)+\frac{\mathrm{d}v}{\mathrm{d}y}=0 \tag{2.1}$$

In relation (2.1) r and y represent radial and axial coordinates, while u and v are radial and axial components of the velocity vector in the fluid film. The axial component of the velocity vector is reduced by integrating the equation (2.1) over the thickness of the material:

$$\int_0^{\mathrm{h}}\frac{1}{r}\frac{\mathrm{d}}{\mathrm{d}r}(ru)=\int_0^{-\mathrm{W}}\frac{\mathrm{d}v}{\mathrm{d}y}\Leftrightarrow h\frac{\mathrm{d}}{\mathrm{d}r}(ru)=rW \tag{2.2}$$

Darcy-Forchheimer model (1.3) characterizes the fluid flow which, for the axial-symmetric model and the notations used, has the form:

$$\frac{\mathrm{d}P}{\mathrm{d}r}=-\frac{\eta}{\phi}u-\frac{C_f\rho}{\sqrt{\phi}}u^2 \tag{2.3}$$

Permeability is determined using the Kozeny-Carman equation written as a function of the local thickness of the porous layer. For the system of equations formed by the relations (2.2) and (2.3) there is no possible analytical solution, and the problem is solved numerically by the finite difference method. Before the numerical solution, the relations (2.2) and (2.3) are written in dimensionless form introducing the following dimensionless variables:

$$\bar{r}=\frac{r}{R};\ \bar{h}=\frac{h}{h_0};\ \bar{v}=\frac{v}{W};\ \bar{u}=\frac{u}{W};\ \bar{P}=\frac{PD}{\eta VR};\ \bar{\phi}=\frac{\phi}{D} \tag{2.4}$$

With these notations, equations (2.2) and (2.3) become:

$$\bar{h}\frac{\mathrm{d}}{\mathrm{d}\bar{r}}(\bar{r}\,\bar{u})=\bar{r}\frac{R}{h_0} \tag{2.5}$$

$$\frac{\mathrm{d}\bar{P}}{\mathrm{d}\bar{r}}=-\frac{\bar{u}}{\bar{\phi}}-\frac{C_f\rho W\sqrt{D}}{\eta\sqrt{\bar{\phi}}}\bar{u}^2=-\frac{\bar{u}}{\bar{\phi}}-C_fK\frac{1}{\sqrt{\bar{\phi}}}\bar{u}^2 \tag{2.6}$$

The parameter $K = \rho W\sqrt{D}/\eta$ in the relation (2.6) is a local Reynolds number, defined according to the characteristic D of the material, which varies with the compression speed W.

Next we consider a network of equidistant nodes, $r_1, \dots, r_{n+1}$. Equations (2.5) and (2.6), discretized using the finite difference method, lead to the relations for the calculation of velocity u and pressure P, necessary for the numerical solution of the proposed problem:

$$\bar{u}_i = \left(\bar{u}_{i-1}\bar{r}_{i-1} + \frac{\Delta\bar{r}}{\bar{h}_j}\frac{\bar{r}_i + \bar{r}_{i-1}}{2}\frac{R}{h_0}\right)/\bar{r}_i \tag{2.7}$$

$$\bar{P}_i = \bar{P}_{i+1} + \left(\frac{1}{\bar{\phi}_i}\bar{u}_i + C_f K\frac{1}{\sqrt{\bar{\phi}_i}}\bar{u}_i{}^2\right)/\Delta\bar{r} \tag{2.8}$$

In relations (2.7) and (2.8) $\bar{u}_i$ and $\bar{P}_i$ represents the velocity and pressure corresponding to each node and j is a counter of the time step. The boundary conditions for pressure are:

$$\partial\bar{P}/\partial\bar{r} = 0, \text{ at } \bar{r} = 0 \tag{2.9}$$

$$P = 0, \text{ at } \bar{r} = 1 \tag{2.10}$$

Considering the continuity equation (2.1) and the boundary conditions for the pressure, the dimensionless flow velocity has a linear variation in the radial direction and reaches its maximum value when the pressure gradient is maximum (at the boundary of the porous disc).

2.2 THE ALGORITHM AND NUMERICAL MODEL VALIDATION

The numerical model was written in the Fortran95 programming language. The solution of the numerical model is performed by the iterative Gauss-Seidel method (without relaxation). The pressure distribution is integrated at each time step, as the dimensionless material thickness is reduced. After obtaining the pressure distribution and flow velocity, corresponding to the modified permeability value, the dimensionless force is determined. The convergence of the algorithm is satisfied if, between two consecutive iterations, the relative variation of a $\bar{F}$ is less than 10^{-9}. The independence of the solution from the nodes is satisfied for $N > 1000$.

Validation of the numerical model is performed by taking the inertial term of the relation (2.8) to be zero. The results are compared with the analytical solution of the dimensionless force (1.7) for the Darcy model (for the same configuration). The variation $\bar{F}$ is evaluated with the relative deformation δ:

$$\delta = 1 - \frac{h}{h_0} = 1 - \bar{h} \tag{2.11}$$

The relative deviation between the numerical and analytical curves is below 0.02%.

2.3 PARAMETRIC STUDY

From the model analysis, the following influence parameters result: Forchheimer coefficient, initial porosity, fluid properties and compression speed. For this parametric analysis, the ratio between the radius of the porous disc and the initial thickness (or relative radius) is $\bar{\rho} = 5$ while the compression velocity is $\mathrm{W} = 1\ \mathrm{m/s}$. The fluid considerer is water, for which $\mathrm{K} \cong 11$. Three values were considered each for C_f (0, 0.2 and 0.3) and for the initial porosity (0.8, 0.9 and 0.95).

2.3.1 Influence of Forchheimer coefficient and initial porosity

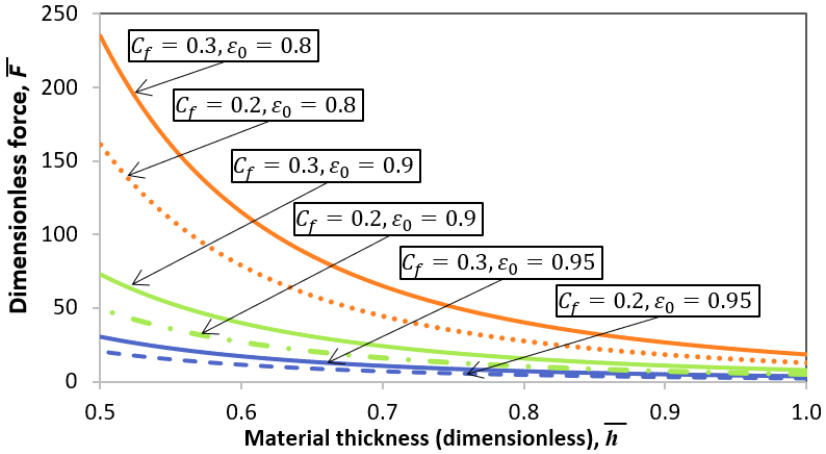

Figure 2.2 Influence of the Forchheimer coefficient and the initial porosity on the dimensionless squeeze force

Figure 2.2 shows that at the same initial porosity (which enters the permeability calculation), the influence of the Forchheimer coefficient cannot be neglected. For the order of magnitude of the chosen Forchheimer coefficients, the pressures in the fluid film increase considerably compared to the Darcy model (for which the maximum value is $\bar{F} < 0.5$). The results for the initial porosity variation (Figure 2.2 and Figure 2.3) show that the impact of the Forchheimer coefficient on the parameters of interest is less than that of the porosity.

Pressure and force values increase with decreasing porosity and increasing Forchheimer coefficient. Regarding porosity, this behavior is consistent with theory.

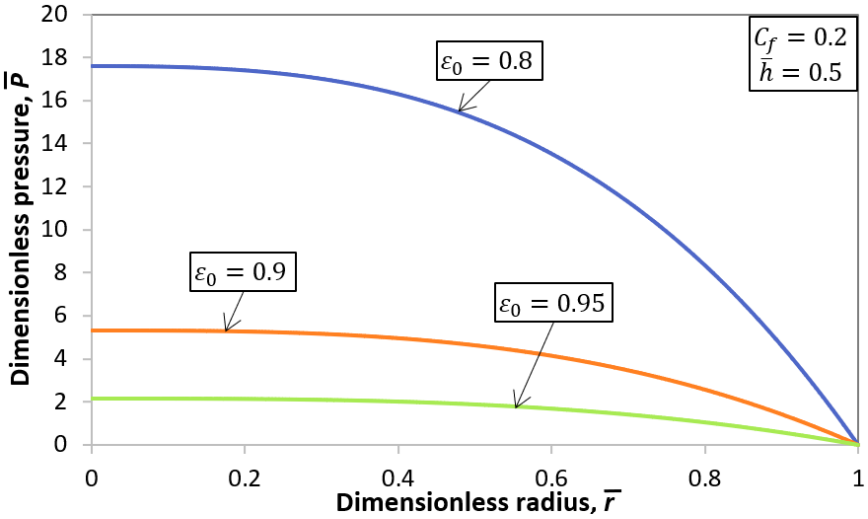

Figure 2.3 Influence of porosity on the dimensionless pressure distribution (Darcy-Forchheimer model)

2.3.2 Influence of fluid and compression speed

A second parametric study was carried out starting from the disc/plane configuration used in article [15] in which a material sample with relative radius $\bar{\rho} = 3.84$ was used. The material used is an S3DU spacer imbibed in glycerine and subsequently subjected to an impact force in order to evaluate the optimal porosity for the considered application. For a compression speed $W = 1\ m/s$, for glycerine one obtains $K \cong 0.015$. For the same speed, a less viscous fluid was also considered, for which we obtain $K \cong 0.07$.

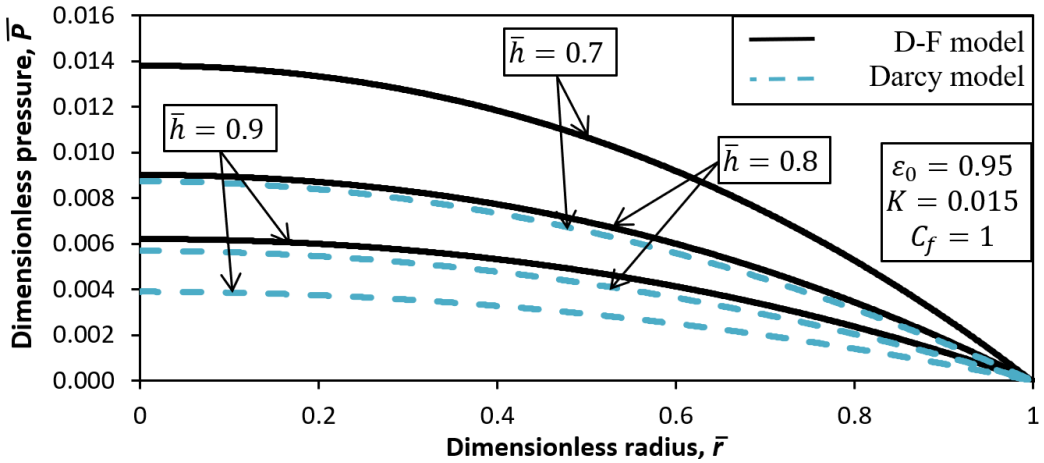

Figure 2.4 Variation of the dimensionless pressure at different values of the dimensionless thickness [58]

In Figure 2.4 the values obtained with the two theoretical models (Darcy and Darcy-Forchheimer) for glycerin are compared at different values of the dimensionless thickness $\bar{h}$. It is noted the increase in pressure generated by the appearance of viscous forces in the fluid film (over 50%). Compared to water, the maximum value of the dimensionless pressure is much lower, although the compression velocities are equal. This is due to the high viscosity of glycerin, which significantly reduces the value of the parameter K($0.015 \ll 11$), which means that higher pressures are needed to achieve flow rates of the same order of magnitude.

From the pressure distribution corresponding to the dimensionless thickness value imposed at the end of compression, the dimensionless force is determined. The influence of inertial effects on it is highlighted by the relative force defined by:

$$\bar{F}_r = \frac{\bar{F}(C_f \neq 0)}{\bar{F}(C_f = 0)} \tag{2.12}$$

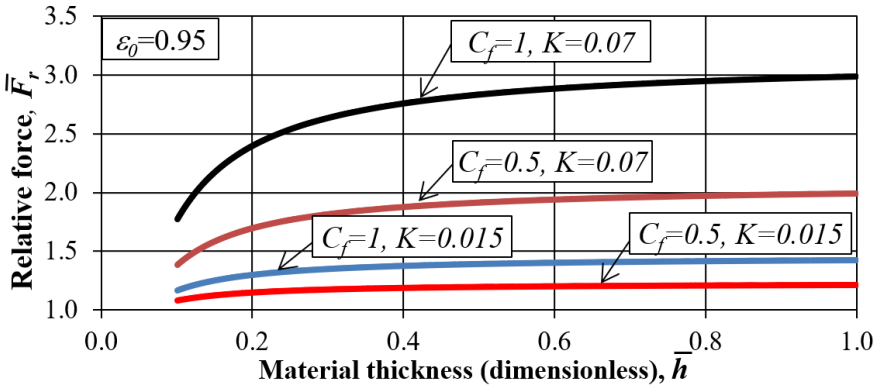

Figure 2.5 Variation of relative force with dimensionless thickness for initial porosity $\varepsilon_0 = 0.95$ [58]

In relation (2.12) the determined forces correspond to the Darcy model ($C_f = 0$) and the Darcy-Forchheimer model. The variation of the relative force is studied for the initial porosity 0.95, two values of C_f (0.5 and 1) and the two analyzed fluids.

Figure 2.5 shows the inertial effects are reducing with the decrease of the porosity during compression. The dimensionless forces obtained with the Darcy-Forchheimer model are higher than for the Darcy case ($\bar{F}_r > 1$), regardless of the values of $\bar{h}$, C_f and K. The increase of the inertial term has a greater influence on $\bar{F}_r$ if the fluid has a lower viscosity The variation of the coefficient C_f is reducing with the dimensionless thickness $\bar{h}$.

2.4 CONCLUSIONS

The results obtained in this chapter show that inertial effects have an important influence on the force and pressure field generated during the compression of an easily deformable porous material. This effect is more visible in the case of high porosity materials imbibed with low viscosity fluids. Another aspect observed is that at high levels of compression, close to the end of the squeeze process, the inertial term tends to lose its effect.

CHAPTER 3
EXPERIMENTAL DETERMINATION OF THE PERMEABILITY LIMIT OF RETICULATED FOAMS WITH COMMUNICATING PORES

From the bibliographic study presented in chapter 1, one of the major problems in the study of flow through porous materials subjected to compression is the definition of the critical porosity, that limit up to which compression leads to the squeeze of the fluid.

In this chapter, a study of the effects of deformations on the porosity of reticulated foams with communicating pores is presented, the interest being the definition of the permeability limit. In order to evaluate the pore volume of the materials, an original experimental device was made, inside which samples imbibed with glycerin were placed. The device was subjected to constant velocity compression on CETR-UMT2 and Zwick/Roell Z010 TN stands.

3.1 THE EXPERIMENTAL DEVICE

3.1.1 Constructive elements

The experimental device (Figure 3.1), a piston-cylinder type, has an open structure at the base that allows the radial flow of the fluid from the porous structure and its separate collection. The dimensions of the slits in the cylinder body have been chosen so that the flow of fluid is as little obstructed as possible.

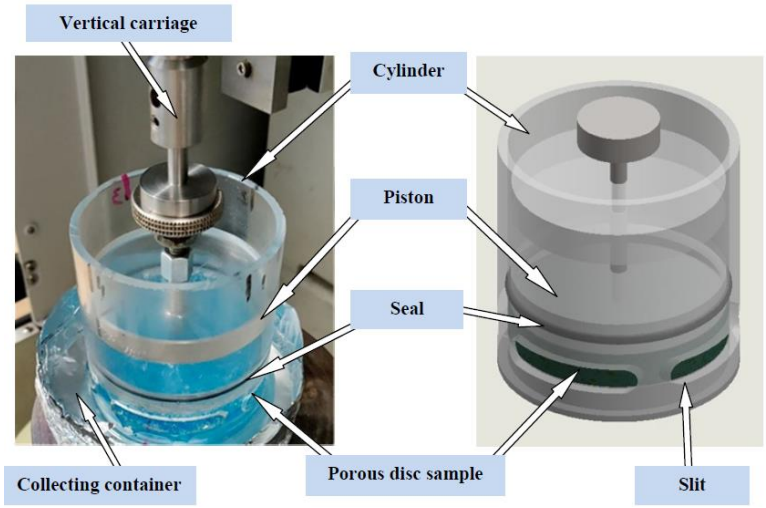

Figure 3.1 Experimental device [94]

On the lower piston disc, an "O" ring prevents fluid from being expelled behind the piston, resulting in a frictional force in addition to the compression force.

3.1.2 Evaluation of friction in the experimental device

On the CETR-UMT2 stand equipped with a force sensor, the frictional force between the "O" ring and the cylinder surface was evaluated. At the same time, the effect of deviations from concentricity and cylindricity was evaluated, in 4 equally spaced positions on the circumference of the cylinder, successively aligned with a mark made on the guide disc.

The influence of the friction force is reduced during the experiments, but a position has been identified where the value is minimal. The alignment of the components was done only in that position and the determined value (10 N) was used to correct the results.

3.2 EXPERIMENTAL PROCEDURE

Disc-shaped material samples ($d = 64\ mm$) of two reticulated foams with communicating pores were tested. The properties of the materials are listed in Table 3.1.

Table 3.1 Properties of material samples tested [94]

Trade Name (Symbol)	Pore size* [mm]	Initial porosity, ($\varepsilon_{0)}$	Initial thickness, ($h_{0)}$ [mm]
FILTREN® TM 25133 (F133)	1.06 ÷ 1.66	0.9854	11.5
FILTREN® TM 25450 (F450)	3.40 ÷ 5.60	0.9870	10.5

* according to the technical sheets of the materials provided by EUROFOAM Romania

The initial porosity of the materials was determined using the volumetric method (with water) described in chapter 1. The testing procedure involves several steps.

A pre-determination of the intrinsic capacity of the materials to retain fluid is necessary to ensure a constant mass of fluid within the pores. It was thus determined that the F450 foam can retain a maximum $32\ g$ of fluid or 72% of the theoretical amount at saturation and the F133 foam retains $45.1\ g$ or 92% of the theoretical value.

Performing a test consists of compressing the sample at a reduced constant speed up to a certain thickness, recording the force and determining the amount of fluid remaining inside, weighing the components in the reverse order of assembly: piston assembly, material sample, cylinder, collecting container. The amount initially introduced must eventually be found in the material or collecting container and on the surfaces of the device. If the losses are greater than 5%, the test is restarted.

The CETR-UM2 stand allows the compression of materials up to thicknesses of 1.5 mm (the limit of 200 N of the sensor is reached). To continue at lower thicknesses ($0.2 - 0.4$ mm) a Zwick/Roell Z010 TN compression machine was used. This also allowed the compression of the dry material to obtain the characteristic stress-relative strain variation curves of the foams.

3.3 EXPERIMENTAL RESULTS

The compression behavior of foams differs according to a series of parameters, presented in chapter 1. In Figure 3.2 you can see the characteristic compression curves of the dry foams, on which the maximum values recorded in the compression tests for successive thicknesses are superimposed. The experimental values closely follow the two curves which shows that the pressure does not appear due to the squeeze effect.

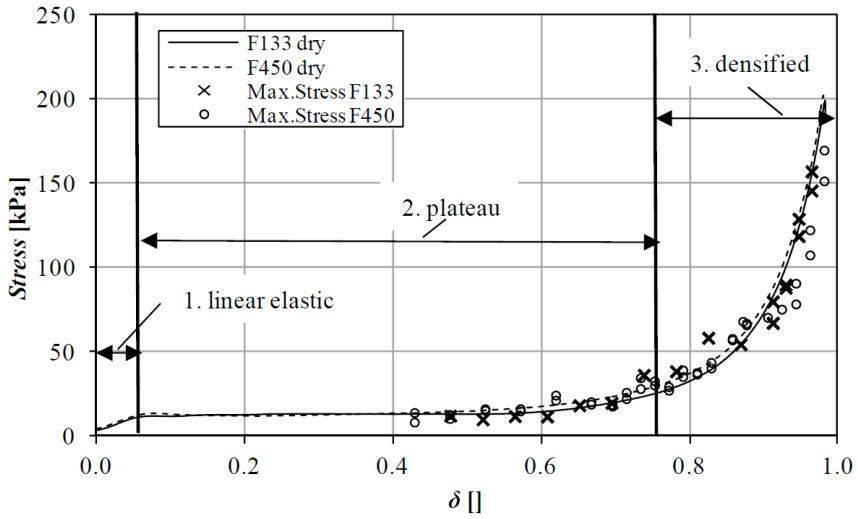

Figure 3.2 Stress-strain curve for material samples (dry and imbibed) [94]

The pore volume as a function of deformation is obtained based on the volume of fluid remaining in the material, accepting the hypothesis that all open pores are occupied by glycerine and that there is no more air inside them.

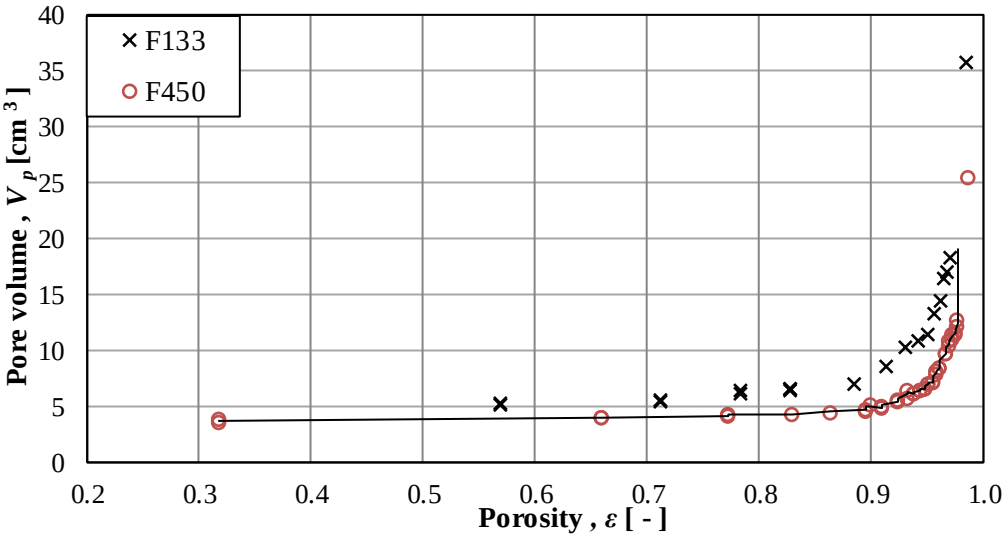

Figure 3.3 Variation of the volume of glycerin remaining inside the structure as a function of porosity [94]

The objective of the study was to determine the critical porosity from which the pores of the materials no longer allow fluid to flow. Figure 3.3 highlights the limit from which the volume of fluid remaining inside the material becomes approximately constant. The porosity variation was determined using the minimum thickness obtained by compression and the relation (1.5). Both materials show asymptotic variations of pore volume with porosity. The studies carried out on the reduced porosity in the densification zone show that, although the materials are compressed far beyond the densification limit, inside the structure a free volume remains unoccupied by the solid matrix, called residual porosity [5]. The values found are around 40% of the initial porosity, but the percentage increases the higher the porosity.

For the analyzed materials, the residual porosity value from which the fluid volume becomes almost constant is $\varepsilon \cong 0.55$ for F133 and corresponds to a compression of the material to a final thickness of 0.4 mm ($\delta = 0.97$). For the less imbibed F450 material, the pore volume approaches 4 cm^3 and the residual porosity value is $\varepsilon \cong 0.5$ (at a thickness of 0.2 mm).

Even if it were technically possible to compress the material to values lower than 0.1 mm (without destroying the device) the volume of fluid remaining inside the pores could not be completely evacuated even if the value is reached $\varepsilon = 0$. The critical porosity at which flow stops completely is estimated in the range $\varepsilon_{cr} \approx 0.1 \div 0.2$.

3.4 CONCLUSIONS

The variations of the compressive stress according to the thickness of the imbibed materials are obtained with the help of an experimental device made especially for these activities. The obtained values are recorded on the characteristic curves of the dry samples, thus succeeding in correlating the mechanical behavior during compression with the degree of absorption. Although the experimental device presents a relatively simple concept, with its help the correlation between the level of compression, the compression force and the volume of the fluid present in the porous layers is highlighted.

The volume of fluid, present even at very high deformations, shows the limit of the XPHD model, since the fluid flow in the material stops before reaching zero porosity, one of the basic assumptions of the theoretical model.

CHAPTER 4
EXPERIMENTAL STUDY OF THE PERIODIC COMPRESSION BEHAVIOR OF RETICULATED FOAMS WITH COMMUNICATING PORES, IMBIBED WITH FLUIDS

The experimental data of the study were obtained on an original bench, specially designed to study the influence of the compression frequency on the characteristics of the fluid film through easily deformable porous materials as well as their reabsorption capacity.

Positive and negative loads are cyclically alternated during the bench's operation. When the surfaces approach in the normal direction, the pressure in the fluid film increases (positive squeeze effect), and when they move away the fluid is reabsorbed into the material generating a suction effect (negative squeeze). During the return phase, under certain conditions, cavitation and even rupture of the fluid film may occur.

No preoccupations have been identified in the literature on the study of fluid-saturated and cyclically compressed porous materials. Therefore, there are many aspects to analyze and investigate to understand the phenomena during compression and decompression as well as how the performances of the fluid film can be controlled. The presented results were obtained during a 5-month Erasmus+ internship held in the Pprime Institute (University of Poitiers, FR).

4.1 THE EXPERIMENTAL BENCH

The main functions of the bench, created in the Pprime Institute, are presented. The personal contribution in the realization of the stand was the identification of the optimal technical solution for the transmission of the periodic compression movement, opting for the use of a cylindrical cam with an internal groove (Figure 4.1 b).

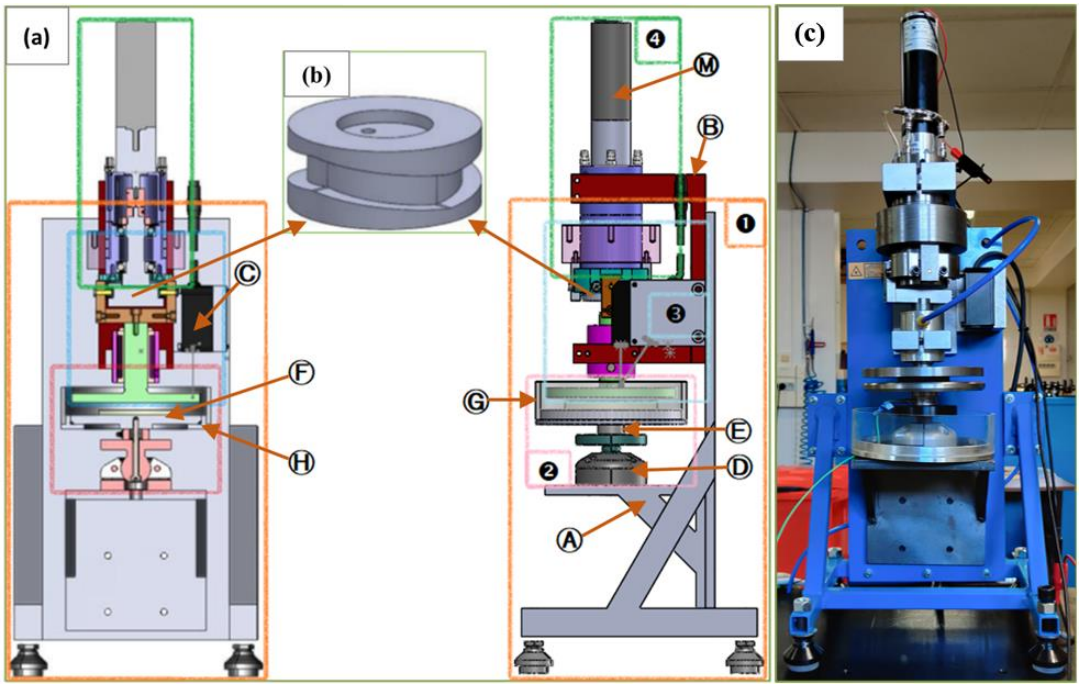

Figure 4.1 Experimental bench: (a) Section view and side view; (b) Cylindrical cam; (c) In assembled condition

This converts the rotation of a drive shaft into periodic motion to actuate the compression plate. The cam was made in two versions: with a compression stroke of 2.2 mm and of 4.5 mm. To achieve high compression frequencies, the cam has a symmetrical profile that ensures two compression strokes during one complete rotation.

The main assemblies of the bench, in the vertical plane (Figure 4.1 a), are the support frame ❶, the fixed plate ❷, the mobile (compression) plate ❸ and the electric motor ❹.

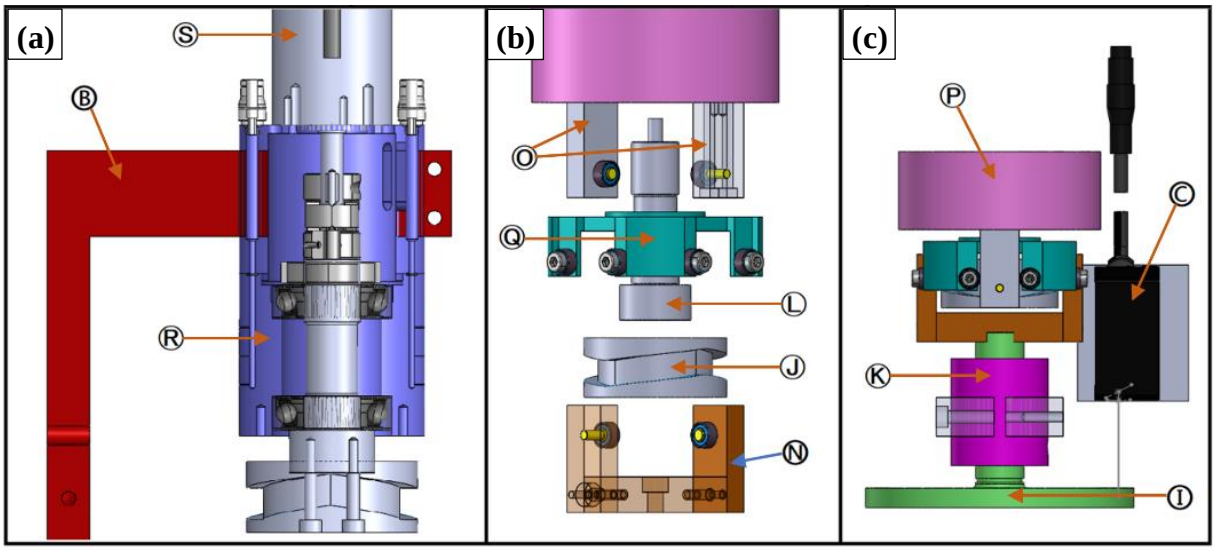

Figure 4.2 (a) Engine assembly section; (b) Motion conversion assembly; (c) Compression plate assembly.

The fixed plate ❷ assembly is supported by a ball joint mounting flange Ⓓ. In the center, this part has a channel that allows the mounting and pretensioning of the axial force transducer Ⓔ, placed between the flange of the ball joint and the fixed plate Ⓕ. A transparent tube Ⓖ mounted on a frame Ⓗ forms the fluid reservoir.

The moving (compression) plate assembly ❸ (Figure 4.2 b and c) contains the top plate Ⓘ, the front cam Ⓙ, the displacement sensor Ⓒ and the plate actuating elements. The rod of the plate is guided by an aerostatic bearing Ⓚ. The front cam is mounted at the end of the driving shaft Ⓛ coupled to the electric motor Ⓜ (Figure 4.2 a).

Two bearings mounted on the fork Ⓝ move the compression plate, guided by the circumferential cam. Simultaneously, another pair of bearings, mounted on two extensions Ⓞ, moves a counterweight Ⓟ in the opposite direction. The movement of the compression plate is registered with the help of the laser beam of the displacement sensor. To ensure translational movement, the fork and the extensions are framed laterally by two bearings, each mounted on the body of the rotation blocker Ⓠ, fixed in the bearing housing Ⓡ of the shaft.

The main function of the measurement and data collection system of the bench is to record the variation of force with compression amplitude and frequency. A Kistler 9031A piezoelectric force transducer was used. The displacement of the compression plate was recorded with the Keyence LK-H050 optical sensor. During the tests, the maximum temperature variation was 1.5°C and the fluid viscosity was considered constant.

4.2 UTILISED MATERIALS

In the test activities three materials were analyzed, the S3DU fabric (presented in chapter 1) and two similar reticulated foams, used in [49] and thereafter referred to as S2404 and S2406. The properties of the two open-cell foams are presented in Table 4.1.

Table 4.1 Properties of reticulated foams used in experiments [49], [1]

Property	Unit	Collar®2404	Collar®2406
Thickness	mm	~ 10	
Compressive strength (40%)	kPa	4.5	5.3 ÷ 6.3
Initial porosity (μCT accuracy 5.74 μm)	–	0.960	0.970
Average pore diameter	mm	0.667	0.549

The tests were performed with two fluids, a synthetic engine oil ($\eta = 0.105\ Pa \cdot s$ at 23°C) and water. The samples tested with oil had the same diameter (60 mm).

4.3 EXPERIMENTAL PROCEDURE

The experimental procedure is described. The voltage of the laboratory supply that feeds the motor is varied to move the compression plate at an imposed frequency. The first strokes are done at low frequencies to remove as much air as possible from the interior and ensure complete saturation with fluid. The repeatability of the results was checked at least three times.

4.4 EXPERIMENTAL RESULTS

The processing of some raw experimental data is first presented.

Compression frequency. The average compression frequency ($\bar{f}$) specific to each acquisition calculated as:

$$\bar{f} = \frac{1}{n}\sum_{n}\frac{1}{T_n} \tag{4.1}$$

In relation (4.1), T is the elapsed time interval between two consecutive minimum (or maximum) points and n is the number of recorded intervals. The minimum value of $n = 5$ to determine the frequency from 2 complete rotations of the cam.

The porosity during testing depends on the level of compression. The maximum (ε_{max}) and minimum (ε_{min}) porosity correspond to the maximum and minimum position of the moving plate during the compression stroke, respectively. Their values are determined from the initial compression of the material (c_0) and the amplitude of the cam (A), using the relation (1.5). The maximum and minimum thickness of the material sample is calculated with the formulas:

$$h_{max} = h_0 - c_0 \tag{4.2}$$

$$h_{min} = h_0 - c_0 - A = h_{max} - A \tag{4.3}$$

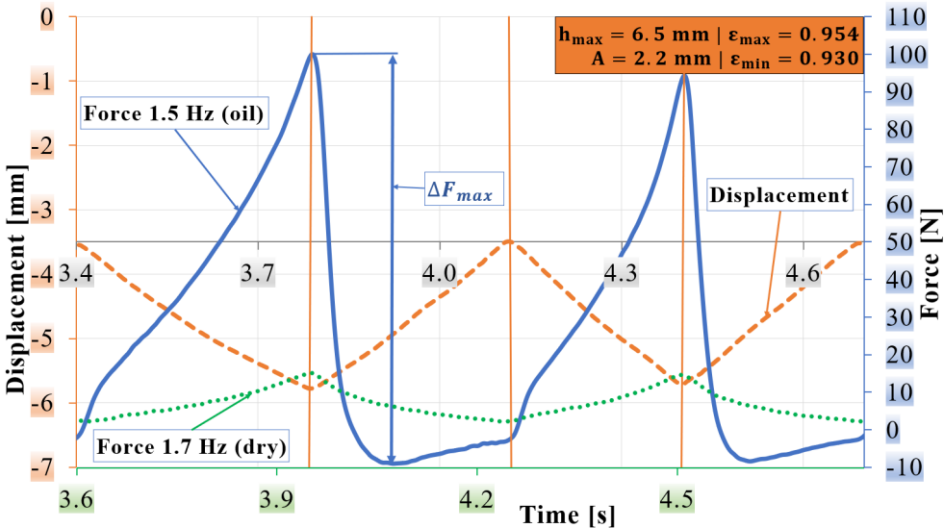

Figure 4.3 Force and displacement variation with time of for an imbibed and dry S2406 foam [56]

Force. In Figure 4.3 Figure the value 0 on the displacement axis corresponds to the initial thickness of the sample (h_0) and the horizontal axis intersects it $3.5\,mm$ below h_0 to mark h_{max}. The effect of imbibing the material is highlighted by showing the variation in force for a sample of dry material. The force profile for the imbibed material, during the return stroke, marks the occurrence of negative force values.

The minimum (negative) value depends on the suction force acting on the radial and on the axial direction. The presence of this resistance to the return movement leads to the sudden decrease in force in the first part. As the fluid is reabsorbed, accumulating in the pores, the force changes from a negative to an increasing (positive) evolution trend before the return of the plate is complete, because the reabsorption process becomes slower than the plate displacement.

Maximum force (pressure). The maximum absolute difference (ΔF_{max}) between the positive and negative force values recorded at a given frequency in an acquisition interval is determined. The material response to compression, recorded as the normal force, is used to later calculate the normal pressure and later ΔP_{max}.

4.4.1 Oil tests

4.4.1.1 The influence of porosity

The porosity and structure of the material influence both the squeeze of fluid from the porous material and the process of re-imbibing with fluid. For the S3DU material, the initial porosity $\varepsilon_0 = 0.907$ and the initial thickness is $6.35\ mm$.

The internal structure of the S3DU material does not create sufficient conditions for the appearance of the XPHD regime under cyclic compression. It is necessary to reanalyze the re-imbibing capacity of this material with another type of fluid. The experimental results with S3DU closed cells showed that the material can be a solution in impact attenuation [15].

Figure 4.4 shows the results obtained for the two oil-imbibed foams, tested under the same conditions as the dry samples. The lower limit of the pressure axis starts from the value of $5\ kPa$ which represents the average value of the pressure obtained on dry samples.

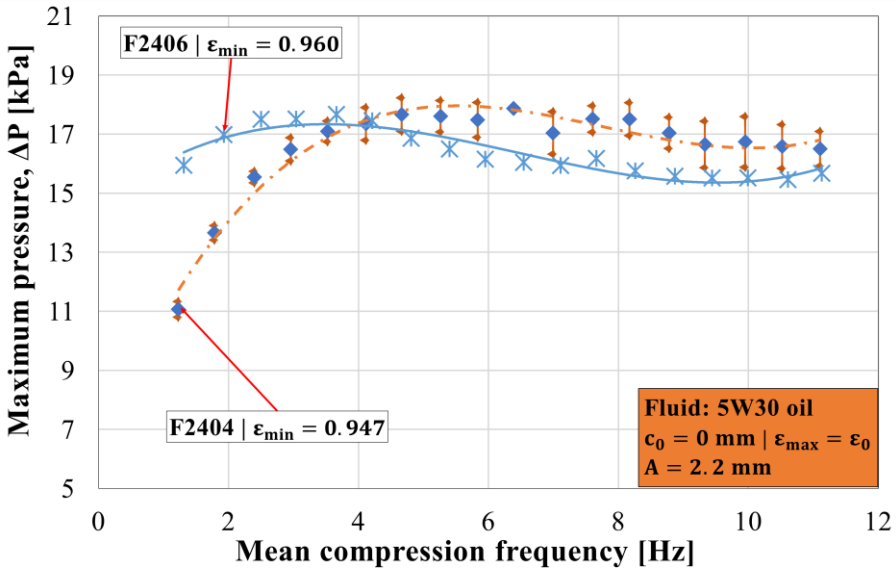

Figure 4.4 Maximum pressure variation with mean frequency for foams with different initial porosities [56]

For S2404, three consecutive sequences are shown, in averaged form, including the standard deviation ($0.5\ kPa$). For the S2406 material the variation of the maximum pressure with frequency is like that obtained for the S2404 foam, but the maximum pressure value is obtained at a lower frequency. Compared to the dry material, the maximum pressures obtained in the case of both foams are $2 \div 3$ times higher.

The difference between the porosities of the two foams (S2404 has the smaller value) in conjunction with the average pore diameter (in this case S2406 has the smaller value) may provide an explanation for the different behavior of the two foams at low frequencies. As the compression frequency increases, both foams begin to behave similarly, as neither of them can fully imbibe.

The results highlight the importance of the material reabsorbing capacity during periodic compression as well as the superior reabsorbing capacity of reticulated foams with compared to S3DU materials. The advantage comes from the internal structure of the foams. These results further show the importance of choosing a suitable fluid-material pair.

4.4.1.2 Influence of cam amplitude and initial compression

Figure 4.5 shows the results of two tests with different amplitudes but the same minimum thickness ($\varepsilon_{min} = 0.926$) for F2404 foam. The variation of maximum pressure with mean frequency is similar. For the cylindrical cam with $A = 4.5\ mm$ the maximum pressures are $6 \div 8$times higher than in the dry case (5 kPa), and for the initially compressed sample and the cam of 2.2 mm, the pressure values are times $5 \div 6$ higher.

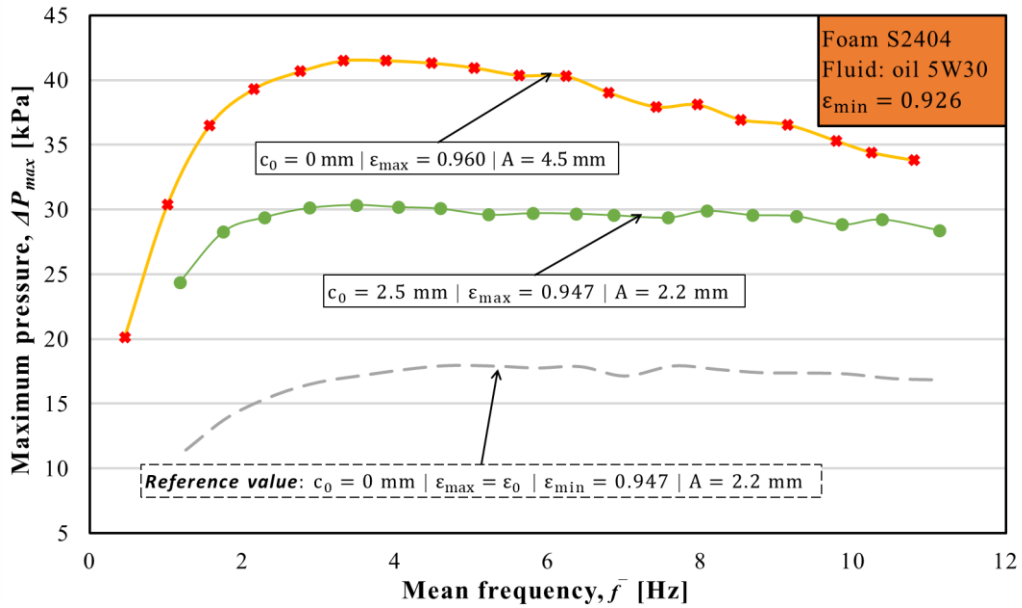

Figure 4.5 Maximum pressure variation with frequency, cam amplitude and initial compression (S2404)

The higher values obtained, with the $4.5\ mm$ cam, can be explained by the fact that, in the middle zone of the foam, more pores remain blocked with fluid, increasing the response of the foam during compression. Another advantage is represented by the fact that the movable plate has a wider stroke which gives the material more time to reabsorb the squeezed fluid.

Figure 4.5 also shows a test done on the same material, compressed with the amplitude $A = 2.2\ mm$, but without initial compression (the configuration shown in Figure 4.4). to compare results obtained at different initial compressions for S2404. It is observed that, when the compression stroke is doubled, the ratio between the maximum pressures obtained in the two configurations is also close to a factor equal to 2.

To study the influence of initial compression on the variation of peak pressure with frequency, tests were made at two new positions of the movable plate (at $c_0 = 3.5\ mm$ and $c_0 = 4.5\ mm$ against the initial thickness) using the $2.2\ mm$ cam on the S2406 foam.

At $c_0 = 3.5\ mm$, the thickness of the S2406 material changes between $h_{max} = 6.5\ mm$ and $h_{min} = 4.3\ mm$. When value $c_0 = 4.5\ mm$ compression occurs between $h_{max} = 5.5\ mm$ and $h_{min} = 3.3\ mm$. The results for these positions are compared with those obtained without initial compression and at $c_0 = 2.5\ mm$. For all the positions, except for $c_0 = 4.5\ mm$, the variation of the maximum pressures with frequency increases with the change of the minimum point of the compression stroke, which influences the minimum porosity reached. For the highest case of initial compression, where $h_{min} = 3.3\ mm$, the pressure variation with frequency increases sharply, being twice as large as the one obtained in the closest position ($h_{min} = 4.3\ mm$), although the change of the minimum point is only $1\ mm$.

The explanation for this sudden increase in the maximum pressure comes from the compression stages of the foams presented in chapter 1. As the material reaches smaller and smaller minimum thicknesses, the pores of the material densify and the applied stress begins to increase to infinity (theoretically). As the specific strain at $h_{min} = 3.3\ mm$ is very close to the value of $\delta = 0.7$, the samples "work" at the confluence between the plateau and the densification stage.

4.4.1.3 Repeatability of results

Experimental results are presented, for five, respectively nine compression cycles made on F2404, respectively F2406 at $c_0 = 3.5\ mm$ with the 2.2 mm cam. For these tests the average standard deviation does not exceed 1 kPa (maximum pressures are in the range $38 \div 42\ kPa$) showing a good degree of repeatability.

4.4.2 Water tests

Using observations from the oil tests, several modifications were made to the bench to ensure a continuous level of saturation of the materials being tested.

4.4.2.1 Modified experimental cell configuration

The piezoelectric force transducer has been replaced by a capacitive one. The fluid reservoir has been modified to provide increased expansion volume during compression. For the same reason, the diameter of the movable plate has been reduced and the thickness of the plate has been increased.

4.4.2.2 Experimental results

Tests were done on S2404 with amplitude cam $A = 4.5\ mm$. Several diameters of porous material discs (98 mm, 105 mm and 130 mm) were tried to obtain the best reabsorbing conditions.

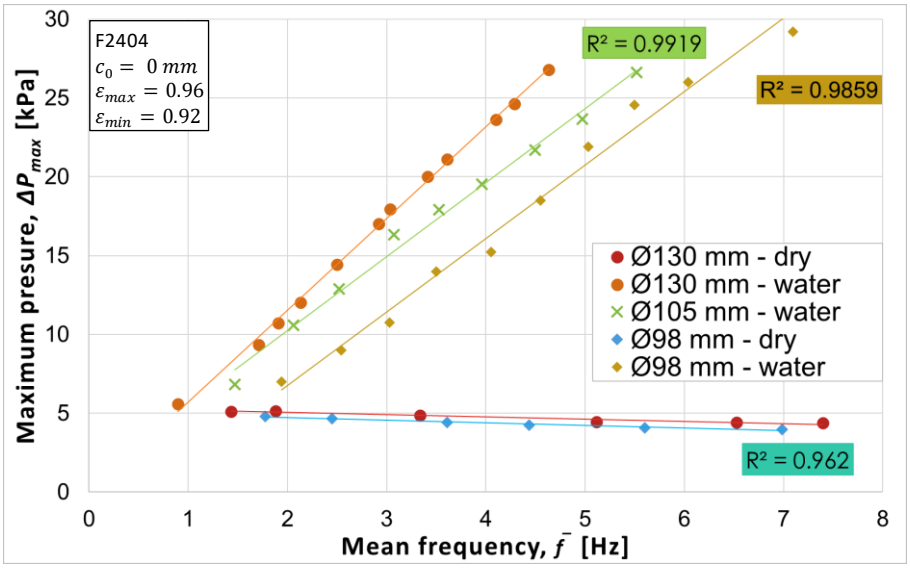

Figure 4.6 Maximum pressure variation with frequency for discs of material with different diameters [16]

In the modified configuration, it was possible to achieve a higher compression frequency $\bar{f} \cong 5.5\ Hz$ only for the foam with a diameter of 98 mm. Figure 4.6 shows that when imbibed

with water, all samples show the same trend of linear evolution of pressure with frequency. For the foam with the smallest diameter this evolution stops at $\bar{f} \cong 7\,Hz$. Above this value, the maximum pressure behaves similarly as in the case of oil imbibition: it enters a small plateau, and above it $\bar{f} \cong 10\,Hz$ it starts to decrease linearly (Figure 4.7Figure).

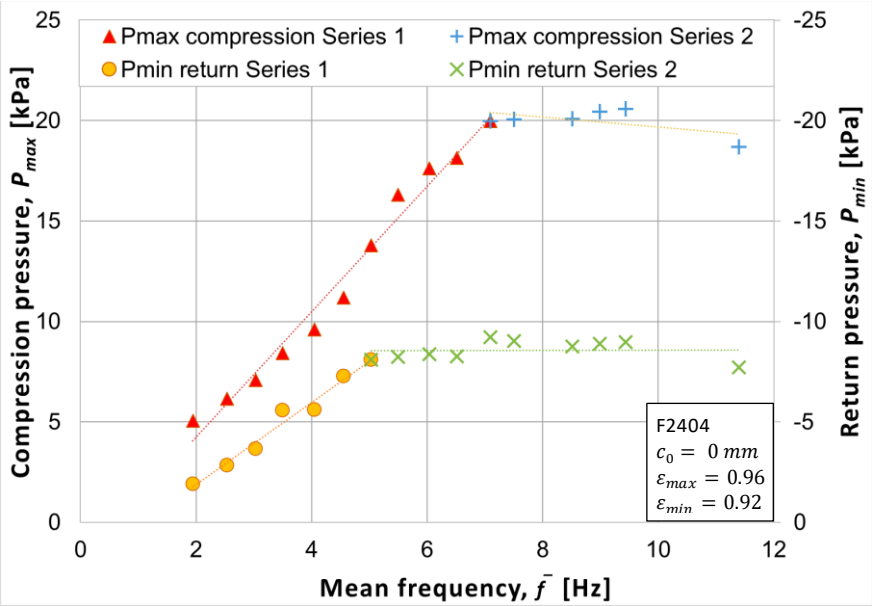

Figure 4.7 Comparison between positive and negative squeeze pressures [16]

Figure 4.7 shows an analysis of the two terms that accumulate in ΔP_{max}, the compression pressure (P_{max}) and the return pressure (P_{min}). The parameters are divided into two series, according to their variation mode. Up to $\bar{f} \cong 4.5\,Hz$, the two pressures have a linear evolution, but different slopes. Around $\bar{f} \cong 5\,Hz$ the pressure P_{min} stagnates while P_{max} continues to increase linearly, until $\bar{f} \cong 7\,Hz$, when it starts to behave similarly to P_{min}.

The reabsorption capacity of the foam after $\bar{f} \cong 5\,Hz$ is limited by a volume of air absorbed during the return stroke, which affects P_{min}. The appearance of air comes from the formation of splashes and waves, due to the cyclic movement of the compression plate. Thus, the foam is no longer permanently surrounded by water and also absorbs air.

4.5 CONCLUSIONS

Material reabsorbing capacity cannot be directly related to porosity, rather it depends on the shape and size of the pores. The frequency of compression influences the reabsorption capacity of the material, the favorable conditions being at lower frequencies. At high frequencies the material fails to absorb enough fluid on the return phase.

When a very low viscosity fluid is used, the maximum pressure increases linearly with frequency (similar to the XPHD regime), over a increased range than with a more viscous fluid. After reaching a limiting frequency, the maximum pressures stagnate, showing similar variations.

CHAPTER 5
NUMERICAL SIMULATION OF THE PERMEABILITY OF A THREE-DIMENSIONAL TEXTILE MATERIAL SUBJECTED TO COMPRESSION

The material chosen for the study presented in this chapter is a 3D Spacer. The activities were conducted during the research internships in the Pprime institute (University of Poitiers) from the periods March-July 2021 and January-May 2023, under the coordination of professors Aurelian Fătu and Yann Henry and through close collaboration with the members of the Lubrication team from PUB. The results presented in this chapter represent an important step in the characterization of textile materials type S3DU used in experimental activities performed over time by the Lubrication team from PUB.

5.1 MORPHOLOGICAL CHARACTERIZATION

The chosen material was previously used by the Pascovici teams in mainly experimental studies ([2], [81], [92], [60]). Hereafter the abbreviation S3DU-H1 is used. The properties of this material, shown in Table 5.1, are taken from the product sheet.

Table 5.1 Material properties S3DU-H1 [3]

Characteristic	Unit	Value	Test method
Mass per unit area	g/m^2	770 ± 30	BS EN 12127
Material thickness (gauge)	mm	6.25 ± 0.5	BS EN ISO 5084
Wales	$number/inch$	16 ± 1	-
Courses	$number/inch$	24 ± 2	-
Compression stress at 40% deformation	kPa	23.81	DIN EN ISO 3386-1

The interest in the characterization of S3DU materials is generally limited to the analysis of mechanical behavior during compressive stresses or the study of air permeability.

The behavior of S3DU in compression is influenced by the initial thickness of the material, the knitting mode of the faces, the diameter, and the angle of inclination of the distancing yarns [54]. It is noted that the information in the technical data sheet is useful, but insufficient for characterizing the material's behavior under compression.

5.1.1 Material determination

To determine the type of polyester used in the manufacture process of the S3DU-H1, threads were extracted from the three layers of the material and analyzed using an infrared spectrometer. Its interface compares the spectrum of materials with existing ones in the integrated library, calculates a degree of similarity (out of 1000 points) and displays the closest spectrum. The highest scores, for the spectra of the three layers, belong to PET.

5.1.2 Outer layers knitting pattern

The density of knitted loops in the faces of the material is an indicator that determines whether the face of an S3DU material has an open or closed type structure [54]. The knitting

patterns of the faces of an S3D material influence the density and distribution of the loops of the middle yarns in the structure and also the structural stability, with implications to the compressive strength. The knitting pattern of the upper face falls into the category of open-type structures, while the pattern of the lower face is specific to a closed-type structure.

5.1.3 Determination of the diameter and tensile modulus for the distancing yarns

The configuration in Figure 5.1 was used to evaluate the diameter and tensile modulus of the distancing yarns, in a process composed of 2 interdependent steps:

1. fixing the distancing yarns and determining the diameter.
2. entering the diameter into the tensile test sequence and performing the test.

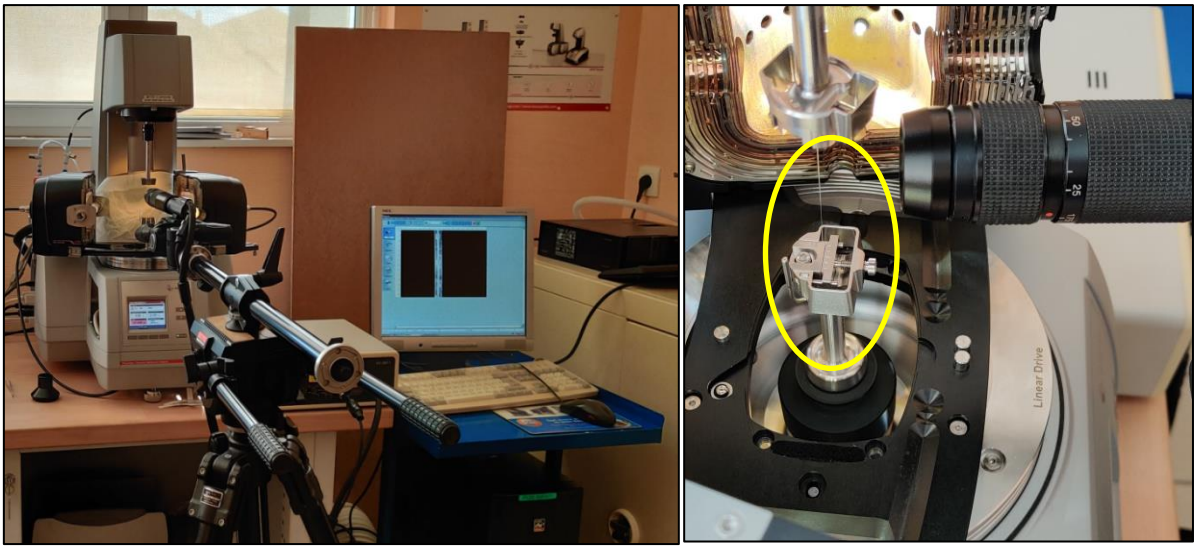

Figure 5.1 Determination of diameter and tensile properties of the distancing yarns of S3DU-H1

5.1.3.1 Description of the experimental setup and procedure

The diameter of the distancing yarns was analyzed with a video-microscope (KEYENCE VH-5911) and two objectives with magnification in the range $25 \div 175X$ and $100 \div 800X$. Image captures of the yarns are made and are processed in Videomet™.

The distancing yarns extracted from the material structure are positioned in a clamping module used in tensile tests performed with the MCR702 MultiDrive platform (Anton Paar). The twisted appearance of the yarns, extracted from the S3DU-H1 structure, is compensated with a pretensioning force ($0.1 \div 0.2N$) to facilitate diameter determination.

From the tensile tests (limited only to the region of linear deformations), the stress-strain curves and the modulus of elasticity of the distancing yarns are determined after processing.

5.1.3.2 Evaluation of mean diameter

The diameter of the distancing yarns has been previously evaluated (by SEM), resulting in an average value of $157.02\ \mu m$ and an apparent diameter[2] of $160\ \mu m$ [2]. These are reference values for method evaluation. The results (with both objectives) were obtained for 15 yarns, for

[2]according to the SR13152:1993 standard

each of which 10 measurements were made along the section. The difference between the results with the two objectives is reduced (Table 5.2).

The relative deviation of the results was calculated from the reference value. By determining the diameter before the tensile test, the specific cross-sectional area of the yarn is more precisely calculated.

Table 5.2 Results obtained for the average diameter of the distancing yarns

175X MAGNIFICATION		**800X MAGNIFICATION**	
Average diameter [µm]	Relative deviation [%]	Average diameter [µm]	Relative deviation [%]
149.08	-5.1	148.69	-5.3

5.1.3.3 Determination of the elasticity modulus

The parameters of the plan chosen for the tensile tests are presented in Table 5.3.

Table 5.3 Program sequence parameters for tensile testing

No. plan	**Yarn pretension**	**Displacement**	**Points recorded**	**Traction velocity**
03/28.05.21	0.2N	0.5 mm	1000	4 µm/s

Upon completion of a test, a curve of force variation with displacement is obtained from which the characteristic curves of the PET yarns are determined in the form of stress-strain. Evaluation of Young's modulus from these curves was performed only on the portion where the stress varies linearly with the strain, approximated by using linear regression curves.

For the approximation to be acceptable R^2 min. 99.95% for min. 400 useful points. The second condition comes from the evolution of the slope of the characteristic curve, different on the portion before the linear variation (the material being still slightly twisted), while on the last portion the slope of the curve changes again because of approaching the elastic limit [84].

Out of 15 yarns subjected to stress, only 10 met both conditions. The results for the tensile modulus and standard deviation can be found in Table 5.4.

Table 5.4 Approximated values of tensile modulus of elasticity and deviation of the results

	Young's modulus [GPa]	**R^2 [%]**	**Number of points [out of 1000]**
Mean value	3.17	99.96	≈ 490
Standard deviation [GPa]	± 0.27	-	-

5.2 DETERMINATION OF MECHANICAL PROPERTIES UNDER CONSTANT VELOCITY COMPRESSION

The study of the mechanical properties of the S3DU-H1 structure was carried out by low-velocity compression tests using the DMA module of the MCR 702 MultiDrive platform.

Table 5.5 Initial thickness of material samples subjected to compression

Test configuration	**I**	**II**	**III**
Initial material thickness [mm]	6,423	6,364	6,443
Relative deviation [%]	≈ - 0.48	≈ - 1.4	≈ - 0.17

The behavior of the S3DU-H1 was analyzed in three different test configurations. The initial distance between the platen of the DMA mode and the sample was chosen depending on

the initial thickness[3] previously determined (6.454 mm [2]). The first cycle of each configuration allowed the evaluation of the initial thickness of the tested samples (Table 5.5).

In the first two configurations the material is compressed by 2.5 mm (39% of the initial thickness) to a final thickness of ~4 mm. In the third test the material is compressed by 4.4 mm (67% of the original thickness) to ~2.1 mm. The compression completion condition of test III is that the maximum force does not exceed the sensor limit (40 N).

After the first compression cycle, the material does not return to its original thickness. The behavior at successive cycles is due to the fact that at deformations greater than 20% the distancing yarns enter an elasto-plastic transition zone (toward the plateau stage) characterized by energy losses through hysteresis, a situation also observed in other experiments [60].

Hysteresis losses are evaluated by determining the energy consumed during compression (E_c), the energy during decompression (E_{dc}), the difference of the two values (ΔE) and the energy dissipated between successive cycles (ΔE_{cs}). The difference is also known as the energy dissipated per cycle [60]. The calculation of energies is reduced to the determination of the area under the curve of variation of force with thickness during the two phases.

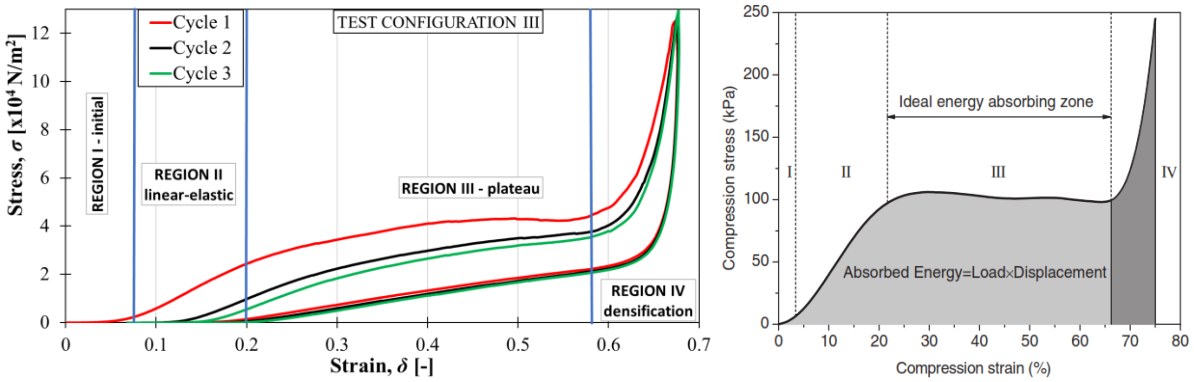

Figure 5.2 Stress-strain curve for S3DU-H1 (left) and characteristic curve for S3D type materials [54] (right)

Figure 5.2 (left) shows the results for test configuration III. The compression speed is 10 µm/s. A 60 s "recovery" pause is made between compression and return. The compressive stress-strain curve specific to S3DU textiles presents four important zones (Figure 5.2, right) detailed in chapter 1. It can be observed that towards the end of compression the material enters densification. Figure 5.2 Figure (left) shows that the sample rapidly loses its elasticity, appearance materialized also in the energy losses centralized in Table 5.6.

Table 5.6 Hysteresis power losses of S3DU-H1 for configuration III

cycle	1	2	3
$E_{c\ III}$ $[10^{-2}Nm]$	4.53	3.34	2.99
$E_{dc\ III}$ $[10^{-2}Nm]$	1.62	1.49	1.43
ΔE_{III} [%]	64.3	55.5	52.2
$\Delta E_{cs\ III}$[%]	-	-13.6	-6

The energy diagrams show the evolution of the absorbed energy per unit volume (W_{abs}) with the normal stress (σ) and is calculated using the relation ([63], [54]):

$$W_{abs} = \int_0^{\delta} \sigma(\delta)\, d\delta \tag{5.1}$$

[3]according to the method described in SR EN ISO 5084:2011

The energy absorption efficiency of a protective material (Eff) shows the ratio between the energy absorbed by a real material, compressed to a certain deformation, and the energy absorbed by an ideal material, which transmits a constant stress equal in value [54]:

$$Eff = \frac{A \cdot h \cdot \int_0^{\delta} \sigma(\delta)\, d\delta}{A \cdot h \cdot \sigma} = \frac{\int_0^{\delta} \sigma(\delta)\, d\delta}{\sigma} \tag{5.2}$$

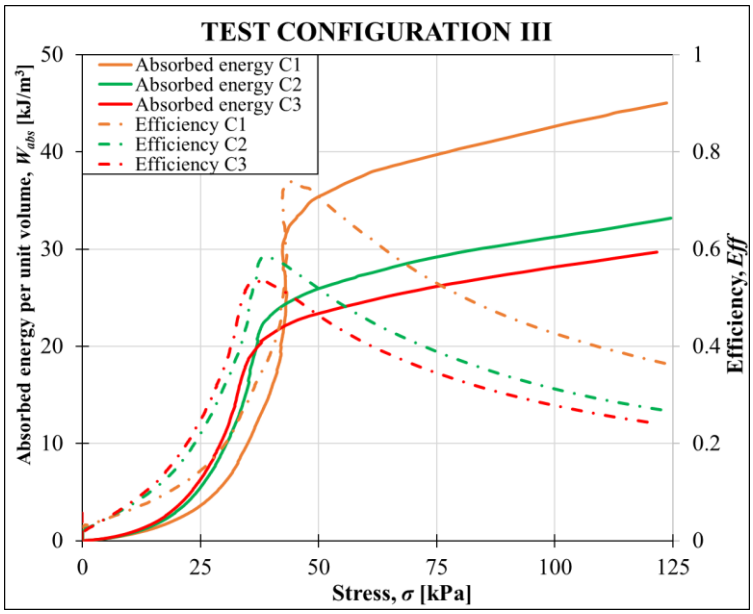

Figure 5.3 Stress-absorbed energy and stress-efficiency curves for S3DU-H1 (configuration III)

The three variation curves $\sigma - W_{abs}$ (for the three compression cycles marked C1, C2 and C3) in Figure 5.3 reveal that the absorbed energy evolves rapidly, and when the stress reaches the plateau area the energy increases suddenly, although the stress remains relatively constant. This stage is followed by a rapid increase in stress with a relatively slow increase in energy. The diagram is useful for optimizing performance or selecting the optimal material for an application, where the allowable stress and the required absorbed energy are defined [54].

The curves $\sigma - Eff$ show a similar trend until the start of densification, with absorption efficiency being maximum at the end of plateau, then gradually decreasing. The maximum of the curve represents a critical point (between stages III and IV), useful for defining the stress in the plateau area, by dividing it by the area of the material [54].

5.3 3D MODELING OF A REPRESENTATIVE CELL

5.3.1 Computer tomograph scanning and processing of the scanned file

Using a computer tomograph (Nikon XT-H225) the micro-tomography of the material was obtained. The good resolution allowed the study of the morphology of the material.

5.3.2 Definition and 3D modeling of a representative cell

The file obtained after tomography is of VISREP type [4] and does not contain information specific to CAD [5] files (of BREP type) and the operations that can be performed on it are thus

[4] visual representation – representation of geometry through polygonal elements
[5] boundary representation – the representation of shapes using their border

limited. The Autodesk Fusion 360 program allows easy switching between the two and was used to group the distancing yarns.

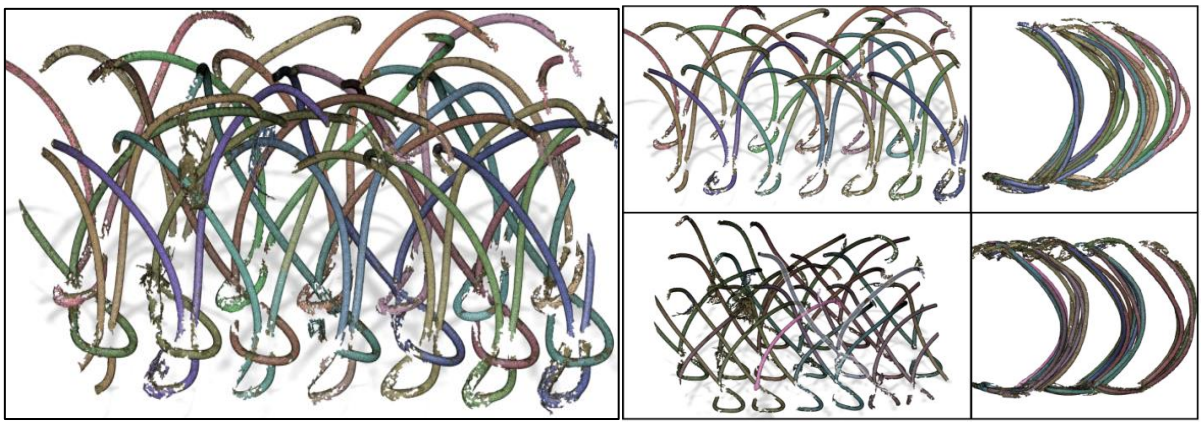

Figure 5.4 Yarn types from the material's structure (Front view and Side view in Fusion 360)

Figure 5.4 shows the way the distancing yarns are knitted in the structure of the material. There are two types of wales that repeat and intertwine alternately.

After separating the distancing layer from the two faces, a representative cell of S3DU-H1 was obtained in the Solidworks CAD program. The simplifications made for its modeling and the lack of information specific to the knitting process limited the parameterization possibilities. The representative cell is composed of four yarns. The yarns were sectioned using planes parallel to the faces, distributed at the points of maximum curvature (of each thread) and near the faces, where a change in curvature is observed (Figure 5.5). By this arrangement of the planes, 5 points are obtained for each yarn, which are joined together to obtain the average fiber.

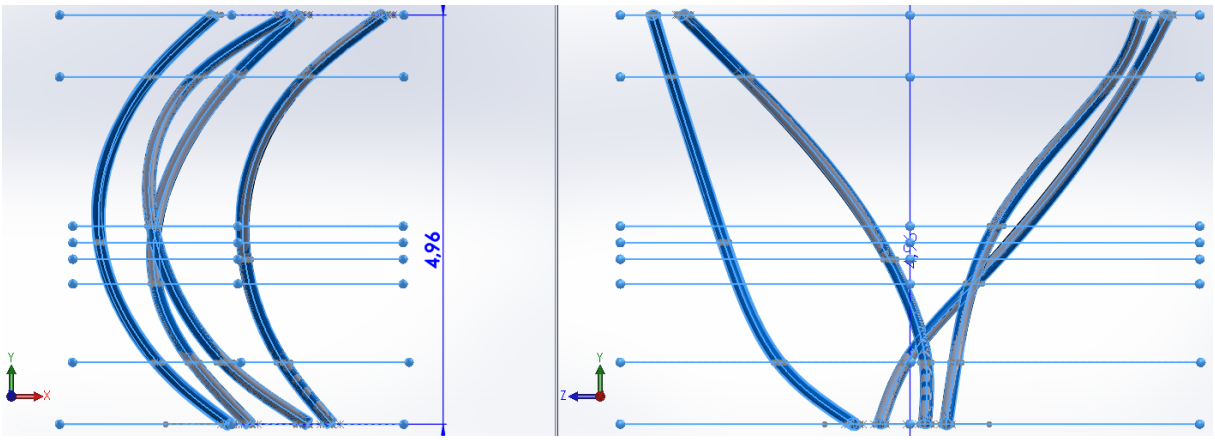

Figure 5.5 Basic elements of the 3D model of representative cell yarns

The final 3D model is obtained by copying the cell in the OX and OZ directions, with a step of 2 mm, respectively 1.575 mm. The values are the average of the (x, z) coordinates of the center of the section area of ten yarns from the scanned file, in the lower plane (at y = 0).

5.3.3 Transferring the solid model to Abaqus program for nonlinear structural analysis

Obtaining the 3D CAD model of the representative cell of S3DU-H1 allows the transition to the study of the compression behavior of the material (made in SIMULIA Abaqus™). Yarns are reconstructed in Abaqus using the previously determined coordinates. The step is also useful

for obtaining a macro command with the help of which new geometries of the yarns or patterns of the representative cell can be quickly generated, by simply changing some parameters.

The geometry of Abaqus finite element models contains the representative cell, multiplied by n times, in OX and OZ, and two thin, rigid plates (the inner surfaces of the faces). It is assumed that the deformation of the faces is negligible with respect to that of the middle layer.

The distancing yarns are meshed with B32 beam elements. Their distribution along the yarns is customized, depending on the length and curvature. Interactions between component surfaces are modeled by two mechanical contact properties, in the directions normal (rigid contact) and tangential to the surfaces. A penalty formulation is used in the tangential direction.

5.4 SIMULATION OF COMPRESSION BEHAVIOR

The results of the nonlinear structural analysis with finite elements are compared with the compression cycle 1 of configuration III (Figure 5.2).

5.4.1 Distancing yarns of equal height

There have been several approaches used to characterize the deformation mechanism of distancing yarns. The best results were obtained with a bilinear elasto-plastic deformation model (the first model was denoted T0).

The model needs the definition of Young's modulus ($E = 3170\ MPa$), Poisson's ratio ($\nu = 0.39$) [6] and the transverse modulus of elasticity ($G = 1140.29\ MPa$), for the elastic portion. For the plastic one, the yield strength ($\sigma_c = 60\ MPa$), the ultimate strength (σ_r) with their deformations (δ_c and δ_r) and the plasticity modulus ($E_p = 0.02E \div 0.04E$) are required.

Starting from the T0 model, a study was carried out on the influence of some parameters on the compression stages II and III, useful for the further evolution of the finite element model. The most important observations of the parametric study are [57]:

- the influence of the friction coefficient between yarns (μ) is reduced.
- the degrees of freedom of the nodes located on the two plates must be constrained.
- yarn's diameter and Young's modulus have the greatest influence on the 2 stages.

In Figure 5.6, the value $\delta = 0.493$ marks both the end of the numerical calculation (performed by the Abaqus standard method) for the analyzed model (T0) and the maximum compression obtained (50% of h_0) with it. The convergence of the model stops at the junction between the plateau and the densification zone, due to the large deformations of the filaments.

The von Mises diagrams show that the maximum stress level of the distancing yarns is distributed in the areas of contact with the plate as well as at the point of maximum curvature. However, the result in the contact area with the plate is influenced by the boundary conditions used. There is a tendency of the yarns to agglomerate in the upper part.

[6] Information extracted from the CES EduPack™ database (v.11.0)

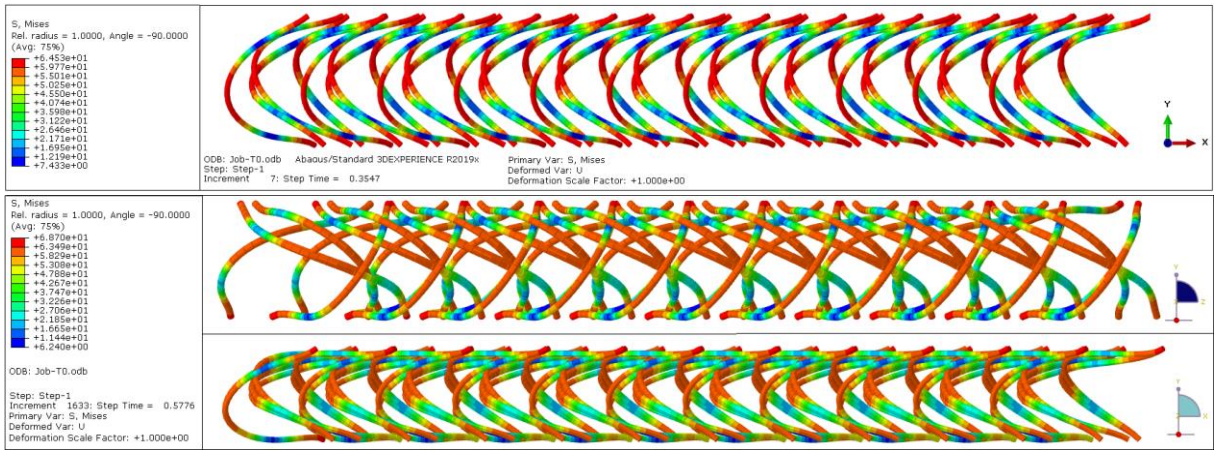

Figure 5.6 von Mises stress diagram (T0) at strain: $\delta = 0.338$ (top) and $\delta = 0.493$ (bottom) [57]

To extend the stress-strain curves obtained by the standard Abaqus method (limited to the plateau stage) the explicit analysis was used. The test conditions are presented in Table 5.7.

Table 5.7 Representative parameters of the numerical models analyzed by the explicit method

No. model	Diameter, (d) [mm]	Yield strength, σ_c (MPa)	Modulus of plasticity, E_p (MPa)	Distance on OZ, (dz) [mm]	Deviation ratio, (h/L)	Yarn height, (Y_{max}) [mm]
T0E1	0.15	60	0.02 · E	1.575	0.1	4.959
T0E2	0.15	60	0.02 · E	1.575	0.01	4.959
T0E3	0.15	60	0.02 · E	1.300	0.01	4.959
T0E4	0.15	60	0.02 · E	1.575	0.1	randomized
T0E5	0.15	80	0.04 · E	1.575	0.1	randomized
T2E1	0.16	60	0.02 · E	1.575	0.01	4.959

Figure 5.7 shows the results obtained for the models with distancing yarns of equal heights. The appearance of the densification stage is observed for all models.

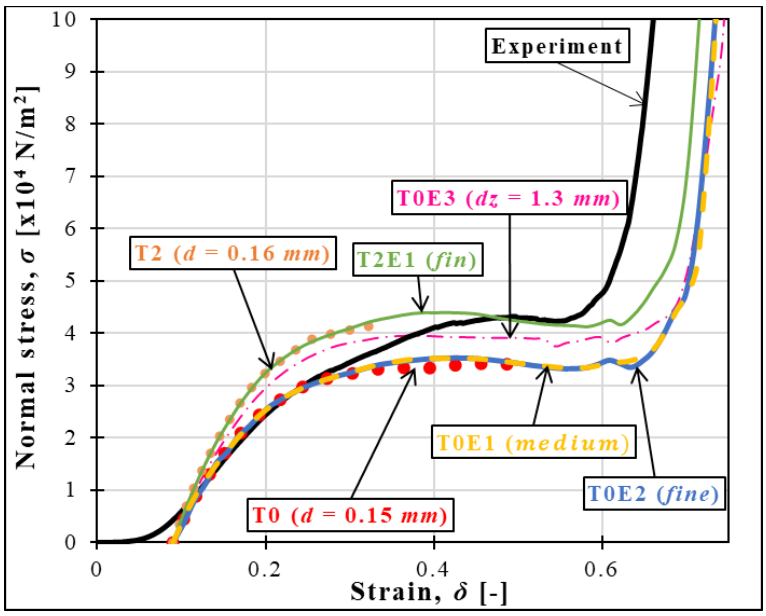

Figure 5.7 Comparison between the experimental and numerical curves of the models with equal height yarns

The numerically obtained curves (Figure 5.7) were moved to the beginning of the linear-elastic stage ($\delta = 0.09$) to correlate them with the experimental results. The height of the distancing yarns in the two faces and the mode of constraint of the multifilament lead to the successive "engagement" of the threads in compression and the occurrence of the initial stage of compression of the material ([54], [40]).

5.4.2 Distancing yarns of different heights

Models T0E4 and T0E5 (Table 5.7) use a randomization function in the Abaqus macro to vary the coordinate $Y_{max}$of the yarns. The function is of the normal distribution type with the mean value equal to the initial value of Y_{max} (4.959 mm) and the standard deviation value equal to the diameter of the yarns. The objective is to characterize the first stage of compression. By introducing small variations in the length of the yarns, the random character of the position of the threads in the structure of the material faces, resulting from the manufacturing process, is simulated. The T0E5 model also contains a plasticity modulus change.

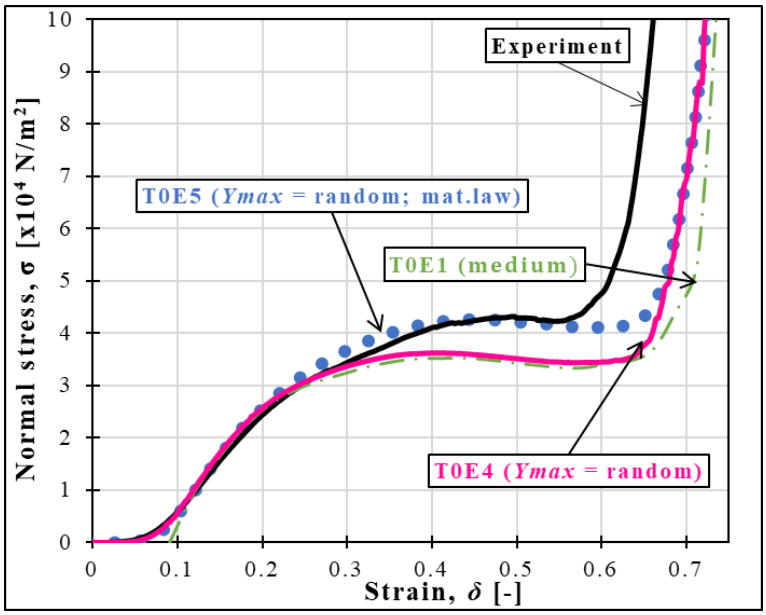

Figure 5.8 Comparison between experiment and numerical models with different yarn lengths

Figure 5.8 shows that this approach allows the characterization of the entire deformation process of the material. The initial stage of the numerical models is overlaid on the experimental result. The T0E5 model faithfully reproduces the first 3 stages of the experimentally obtained curve. The densification behavior is close to the best result obtained (with the T2E1 model).

5.5 SIMULATION OF THE FLOW OF A NEWTONIAN LIQUID THROUGH THE REPRESENTATIVE CELL

The main objective is to determine the permeability variation with the compression level of the material. Permeability is determined with the theoretical Darcy model, at low flow velocities, by applying a pressure difference between the boundary surfaces in the flow direction. Another objective is to test the applicability limit of the laminar flow model and compare the results with more complex theoretical models derived from Darcy's law.

5.5.1 Transferring the finite element model to Ansys Fluent

The deformed shape of yarns from Abaqus, at successive compression levels (files with the extension *.rpt*) are exported. Through a Fortran routine, Abaqus files are converted to *.dat* files. These are imported with a macro into *Catia* and processed to obtain, through a Boolean operation, the "negative" of the deformed threads (the pore volume). The plane dimensions are

those of a representative cell (2 mmx 1.575 mm) and the height depends on the deformation level of the model in the file exported from Abaqus.

5.5.2 Description of models made in Fluent

Simulating a Fluent model requires specific steps. The STEP files (from *Catia*) are imported into the Design Modeler module where the boundary surfaces of the volume are selected and named. The name of the surfaces is given by the main axes normal to them and the indices min and max which indicate the proximity of the surface to the origin of the coordinate system. The geometry is meshed with an unstructured model with tetrahedral elements, and in the definition stage of the analysis, these are converted into polyhedral/polygonal elements.

The laminar flow model is used. The influence of viscosity on flow was analyzed with two fluids: water and glycerin. The conditions for surfaces are: Z_{min} and Z_{max} are interfaces with "periodic boundary condition" and Y_{min} and Y_{max} they are impermeable walls with a "no-slip" condition. Two models are analyzed for the flow direction. In the first (denoted PB) it is used for X_{min} and X_{max} the condition used for Z_{min} and Z_{max}. This approach allows the input of a pressure gradient in the flow direction, directly from the operating conditions (în Pa/m).

In the second model (noted PO) "pressure outlet" conditions are imposed for X_{min} and X_{max} and a static pressure difference is created (on one of the surfaces $P \neq 0$ and on the other $P = 0$). The solver will automatically reverse the flow direction, from high to low pressure.

An algorithm in which the pressure is coupled with the flow velocity is used and the flow is considered pseudo-transient. In the CFD post-analysis, the average velocity over the area of the flow surfaces and the integral of the average velocity are determined to obtain the flow rate.

5.5.3 Numerical evaluation of the permeability of S3DU-H1 material

The study of the quality of the models made reveals a minimum level of residuals of 10^{-6} and an average mesh of the model, for a balanced calculation time with good accuracy.

5.5.3.1 Comparison of models made with different fluids and boundary conditions

Several preliminary model checks were performed. The influence of boundary conditions on the results is most important, especially in the main flow direction. The two numerical models with different boundary conditions were verified over a wide range of pressure gradients. The obtained results were differentiated according to the variation of the mean velocity with the pressure gradient, linear or non-linear.

For this study, the cell with non-deformed yarns was used. For the case of linear variation of mean velocity with pressure gradient, Darcy's law is written in the equivalent form:

$$\frac{\partial p}{\partial x} = \frac{\eta}{\phi} u_{medie} \Leftrightarrow \frac{\Delta P}{L} = T_{Da} \cdot u_{med} \tag{5.3}$$

In relation (5.3) the parameter T_{Da} considers the effects of viscosity and has the geometric meaning of the slope of the variation line between ∇P and u_{med}. Permeability results from:

$$T_{Da} = \frac{\eta}{\phi} \rightarrow \phi_{Darcy} = \frac{\eta}{T_{Da}} \tag{5.4}$$

The variation of u_{med} with the imposed pressure gradient is analyzed with the LINEST function (Excel). The linear regression function approximates the numerical data very well (Figure 5.9).

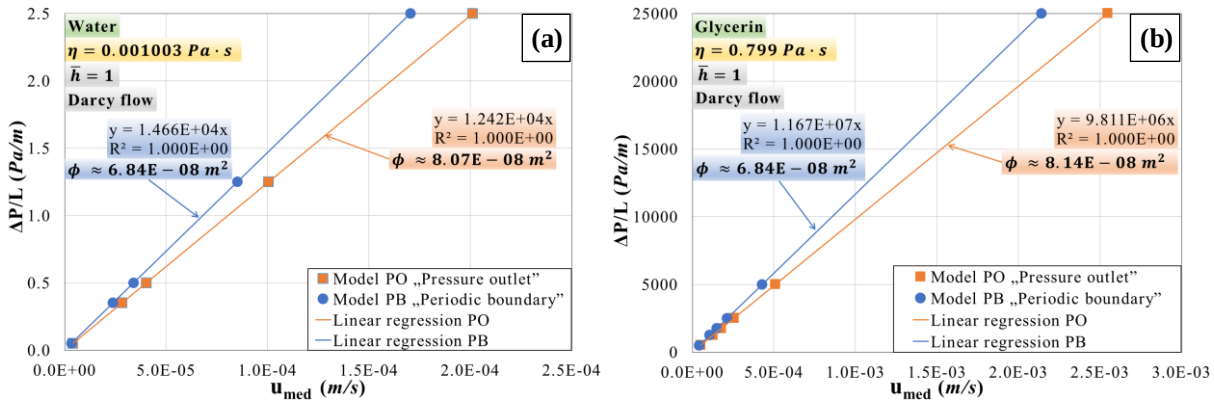

Figure 5.9 Linear variation of calculated u_{med} with imposed ∇P for: (a) water (b) glycerine

Figure 5.9 shows that the permeability of the material depends on the boundary conditions used, the difference between the two models being about 16%. The results are independent of the analyzed fluid and the permeability difference under the same boundary conditions is negligible. Fluid viscosity influences the order of magnitude of flow velocities.

Increasing the pressure difference applied to the two models, it is observed that the fluid velocity leaves the zone of linear evolution. Figure 5.10 shows the flow velocities obtained for the two fluids at increased pressure gradient values.

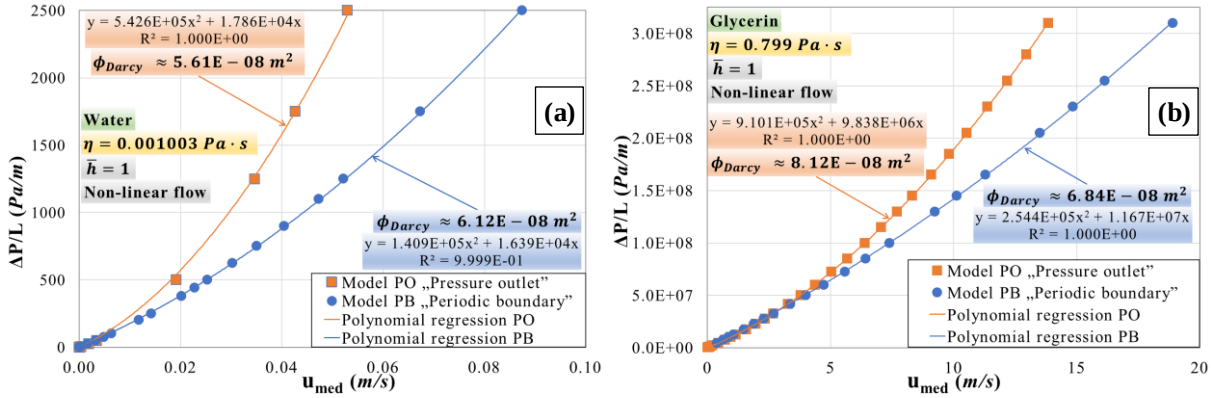

Figure 5.10 Non-linear variation of calculated u_{med} with imposed ∇P for: (a) water (b) glycerine

The new curves ∇Pand u_{med}were approximated by quadratic polynomial trend lines. The curves show different evolutions for the two fluids, more visible for water (ϕ_{Darcy}reduces by 45%). The influence of viscosity begins to decrease with increasing flow velocity, leading to a non-linear evolution with the imposed pressure gradient. Important differences in the results of the two models were further investigated.

5.5.3.2 Verification of boundary conditions for the case of flow through a pipe

The verification was carried out on a simple model of a pipe with a length greater than the diameter. The evaluation of the numerical results was carried out with the analytical solution for flow of the Hagen-Poiseuille equation. The results obtained for the two models were verified at three values of ΔP. The results with the PB model lead to numerical solutions very close to

the analytical ones. The PO model reduces the flow rates and flow velocities as the imposed difference between inlet and outlet pressure increases.

5.5.3.3 Influence of the number of representative cells

The PO model was verified on two geometries with different lengths of the flow domain in the direction OX. The two analyzed geometries contain five (PO 5X) and respectively ten representative cells (PO 10X) along the flow domain. The analysis of the new PO models was performed at three different pressure gradient (with glycerin) and the results were compared with those obtained at the same pressure gradient with the PB model (reference value).

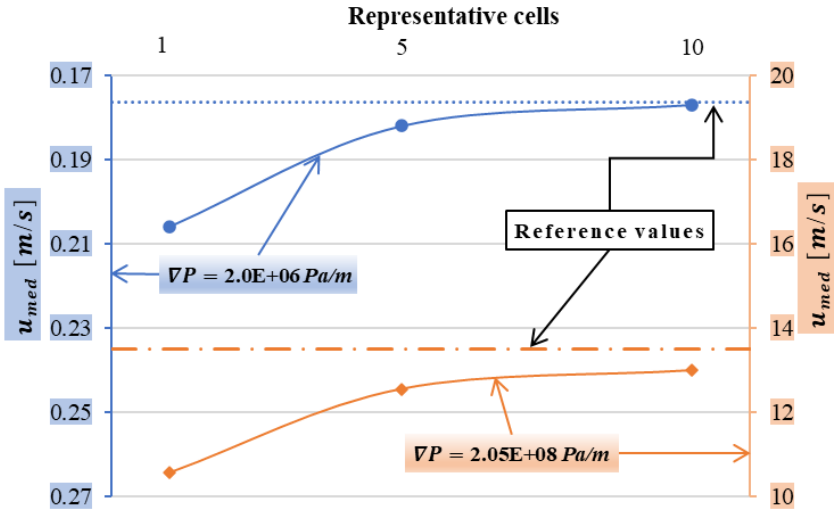

Figure 5.11 Variation of mean velocity with the number of representative cells

Figure 5.11 shows that the solution of the modified PO numerical models approaches the solution chosen as reference (the PB model) as the number of representative cells increases. The improvement means a substantial increase in computing time.

5.5.4 Permeability analysis using the Dupuit-Forchheimer extension of Darcy's law

Several approaches were used to analyze the permeability of the data set obtained from the values of the imposed pressure gradient and the numerically calculated flow velocity. In a first approach, the permeability was determined from Darcy's law for each point, analyzing the evolution with the flow regime (Re_ϕ) The permeability, with both fluids, decreases with the increase of the flow regime by approximately 50%.

The following approaches involved the determination of permeability using polynomial regressions (of the second degree) to verify the theoretical flow model described by relation (1.3). The working method proposed in [4] involves writing the relation (1.3) in the form:

$$\frac{\Delta P}{L} = T_{Da} \cdot u_{med} + T_{Fo} \cdot u_{med}^2 \tag{5.5}$$

$$T_{Fo} = \rho \frac{C_f}{\sqrt{\phi}} = \rho \cdot C \tag{5.6}$$

The term T_{Fo} is the Forchheimer term. Putting the equation (1.3) in the equivalent form, T_{Da} and T_{Fo} is determined by the least squares method ([4], [10]). To evaluate the deviation

between the approximation curves and the points obtained numerically, the mean deviation of the pressure difference ($\overline{\Delta P}$) and the relative mean deviation of the data ($\overline{Err}$) are used.

Several approaches are used to obtain polynomial regression curves. In the first approach (denoted $\phi = \text{const}$), the permeability is determined from the zone of linear variation. The approximation of the data is done on the points that no longer respect the Darcy model. The approach leads to results similar to the one in Figure 5.12 ($\overline{Err} = 1.1\%$).

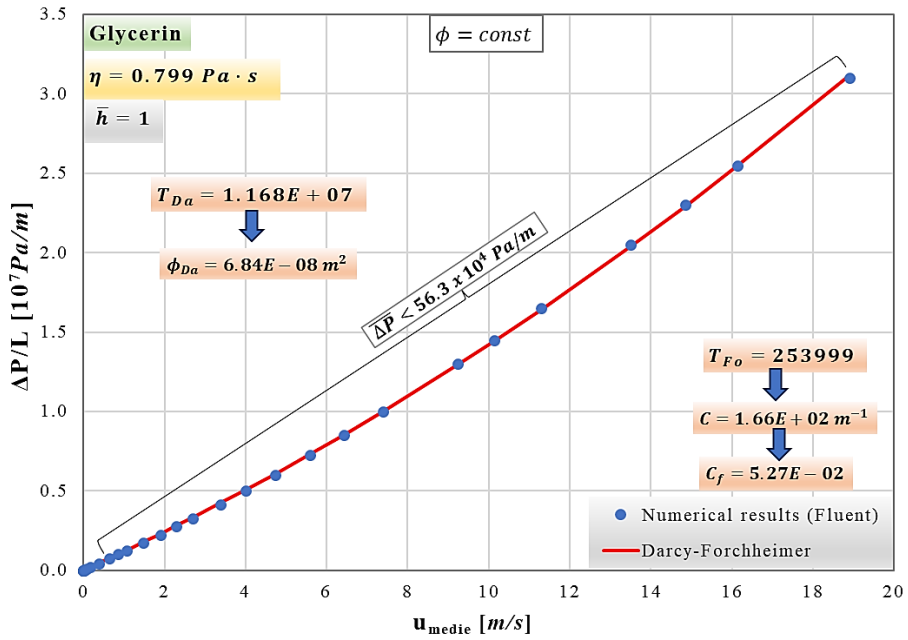

Figure 5.12 Variation of flow velocity with pressure gradient (glycerin) –Darcy-Forchheimer ($\phi = const$)

The second approach involves approximating numerical data by polynomial regression curves for a range of flow velocities ($D - F_{interval}$) or for the entire data set ($D - F_{tot}$). The best approximation of the data is obtained by the method $\mathrm{D - F_{interval}}$, which involves the determination of T_{Da} and T_{Fo} by least square method for all values up to a certain flow velocity value. Obtaining them allows the calculation of the permeability and form drag coefficient (C) or the Forchheimer coefficient (C_f) related to the curve delimited by the verified flow velocity value. This method was also successfully used in [4] and allows the analysis of the variation of the permeability and of the coefficients C or C_f with the flow regime.

By this approach, the deviations of the results obtained for water are $\overline{\Delta P} = 1.95\ Pa/m$ and $\overline{Err} = 0.17\%$ and, for glycerin, $\overline{\Delta P} = 1.4 \cdot 10^5\ Pa/m$ and respectively $\overline{Err} = 0.08\%$. Compared to the method, $\phi = const$ these results represent an improvement of approximately 90% of $\overline{\Delta P}$ and $\overline{Err}$. In contrast to using the theoretical Darcy model to approximate the data, with the Darcy-Forchheimer model the permeability is reduced by only 11%.

Figure 5.13 shows the same variation of ϕ and factor C obtained with the two fluids and that their values are not constant. The components of the Darcy-Forchheimer model change with different slopes depending on the dominant characteristic of the flow regime. In the linear zone, the permeability is relatively constant and the factor C shows small oscillations of the values (because a linear data set is interpolated with a second-order polynomial [4]). In the transition zone between the regime dominated by viscosity (linear) and that dominated by the form drag coefficient (inertial effects), ϕ and C increase reaching a maximum at $Re_\phi \approx 3.1$.

After reaching the maximum point, the permeability tends to decrease with the increase of the flow regime, and the coefficient C tends to stabilize in the range of 125÷150 m^{-1}.

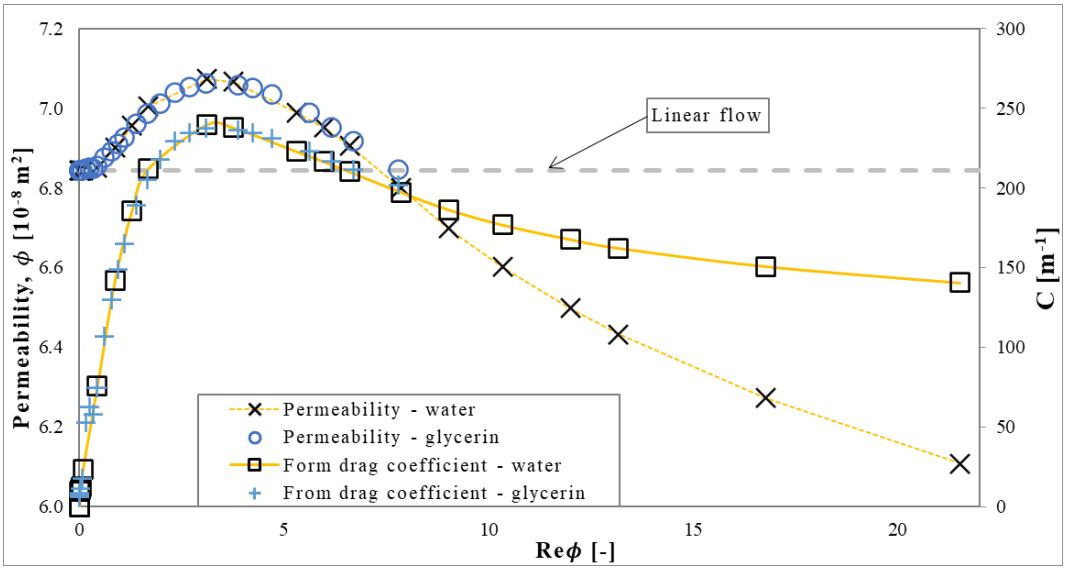

Figure 5.13 Permeability and form drag coefficient variation with flow regime – Darcy-Forchheimer model, least square method applied on intervals

Following the permeability variation, from the data obtained for water, the limit of the Darcy model was identified, depending on the flow regime. The zone $Re_\phi = 0.1 \div 3.5$ is the transition zone between the Darcy flow to the Darcy-Forchheimer model. The upper limit of the transition regime is close to that identified in the study [30] where a similar numerical study was carried out.

5.6 COMPARISON OF CALCULATED PERMEABILITY WITH EXPERIMENTAL RESULTS

The PB (imposed pressure gradient) model is used to analyze the variation of permeability with strain. The numerical results were compared with experimental measurements with glycerin made on the same material by C. Enescu [27].

Permeability from numerical data was determined using Darcy's law and low-value pressure gradients. Yarn shapes at different compression levels were extracted from the Abaqus T0E1 model to perform CFD analysis on a representative cell. Although the T0E5 model showed the evolution closest to the experimental stress-strain curve, the variation in yarn height does not allow the use of a single cell.

The initial porosity ($\varepsilon_0 = 0.9694$) was determined from the geometric model and its variation with the compression level was realized using the solid fraction conservation equation. The porosity of the representative cell represents the ideal porosity of the middle layer. The faces of the material reduce the experimentally determined values (0.91÷0.95), but an experimental evaluation of the porosity of the middle layer of the material is not possible.

The permeability was evaluated in the plane flow directions (OX and OZ) which is why the resulting permeability was also determined ϕ_R, as follows:

$$\phi_R = \frac{1}{3}\phi_{OX} + \frac{2}{3}\phi_{OZ} \tag{5.7}$$

Table 5.8 Permeability of the deformed volumes of distancing yarns

Numerical model height, Y_{max} [mm]	Deformation value [mm]	Equivalent thickness S3DU-H1, h [mm]	*Porosity ε [–]	ϕ_{OX} [m²]	ϕ_{OZ} [m²]	Permeability difference [%]	ϕ_R [m²]
4.959	0	6.454	0.9694	6.84E-08	6.59E-08	3.76	6.67E-08
3.957	1.002	5.452	0.9617	4.71E-08	4.76E-08	-1.03	4.74E-08
2.955	2.004	4.450	0.9487	3.51E-08	3.45E-08	1.64	3.47E-08
2.454	2.505	3.949	0.9382	2.87E-08	2.72E-08	5.48	2.77E-08
1.953	3.006	3.448	0.9223	2.13E-08	1.86E-08	12.49	1.95E-08
1.452	3.507	2.947	0.8955	1.16E-08	9.45E-09	18.24	1.02E-08
1.202	3.758	2.697	0.8737	8.52E-09	5.70E-09	33.12	6.64E-09
1.035	3.925	2.530	0.8534	6.49E-09	3.69E-09	43.22	4.62E-09
0.951	4.008	2.446	0.8405	5.75E-09	3.20E-09	44.28	4.05E-09
0.751	4.208	2.246	0.7979	3.54E-09	2.01E-09	43.18	2.52E-09

**In the calculation of the equivalent thickness, the two parallel faces, that add up to a thickness of 1.495 mm, were considered*

Table 5.8 shows the calculated permeability values at different strain levels. Using this data, Figure 5.14 shows the variation of permeability with porosity during compression.

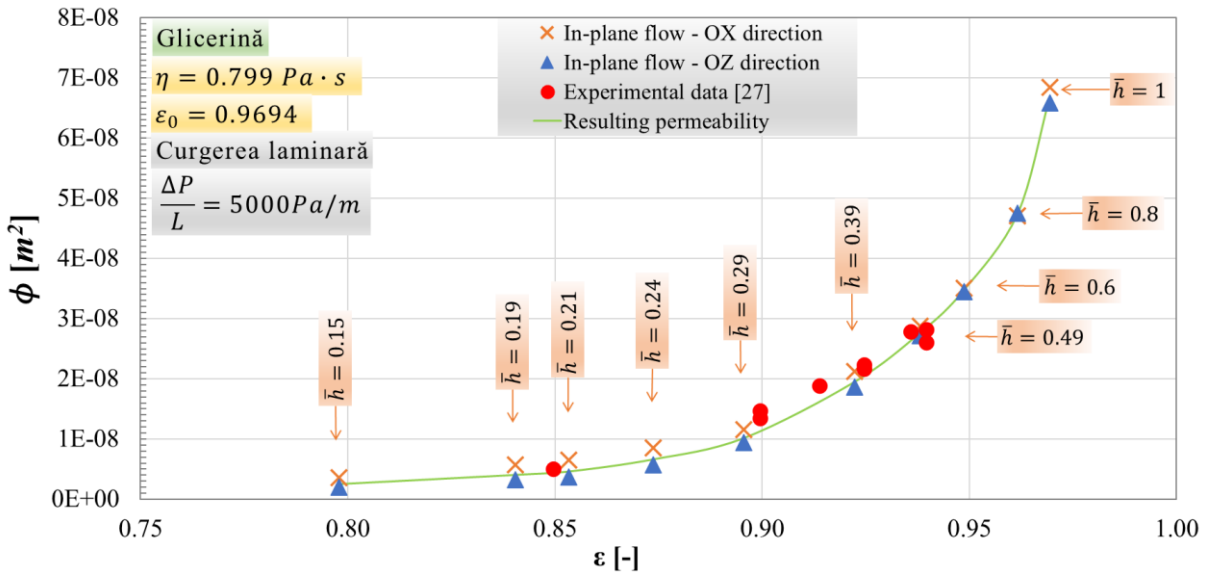

Figure 5.14 Variation of numerical model permeability with porosity

Figure 5.14 also shows the comparison of the results obtained numerically with those determined experimentally by C. Enescu [27]. The graph shows that the experimental results are very close to those obtained by CFD analysis. It is observed that the experimental values of the permeability of the material (including both sides) is dominated by the permeability of the distancing layer. The assumption is valid if the outer layers do not come into contact.

For higher values of the porosity, there are no experimental results because the flow rates are very high and the construction of the permeameter does not allow the collection of the fluid. Considering all the simplifications, the results obtained from the CFD analysis show a very good level of correlation with the experimental data.

5.7 CONCLUSIONS

The variation of permeability with porosity, at different levels of compression and for pressure gradients with low values, obtained numerically in a CFD environment shows a very

good level of correlation with the data obtained from experimental measurements, under the same conditions. The results show the usefulness of the analysis method for compressive permeability assessment.

A limit of the linear flow through the representative undeformed cell was successfully determined. The numerical results obtained for two fluids used show that the permeability of the material does not depend on the fluid used.

For the analyzed flow domain ($Re_\phi < 23$), the Darcy-Forchheimer model provides a good approximation of the data. Data processing shows a variation of permeability with flow regime, consistent with observations found in the literature for flow models using flow resistance theory.

CHAPTER 6
GENERAL CONCLUSIONS. PERSONAL CONTRIBUTIONS. FUTURE DIRECTIONS OF RESEARCH

6.1 GENERAL CONCLUSIONS

- The main problems that appeared in the studies dedicated to the mechanism of the squeeze of fluids through highly compressible porous media, revealed a series of discrepancies that appear especially at high speeds specific to impact applications, where theoretical models based on Darcy-type flow become less accurate. Other possible sources identified, such as the closing of the communicating pores before zero porosity is reached or the permeability values determined experimentally, difficult to correlate with others obtained under similar conditions, led to the reconsideration of some of the simplifying assumptions that were the basis of the XPHD mechanism.

At the same time, the promising results obtained in impact attenuation, highlighted theoretically and experimentally, led to a special interest in expanding the use of the XPHD mechanism for the case of repeated (oscillatory) movements through successive impact. In contrast, in the case of cyclic movements specific to long-term or multiple-use applications, the XPHD mechanism has yet to be explored.

The listed reasons substantiated the main directions addressed in this work.

- When the Reynolds number, calculated for flow through porous media, exceeds a value specific to the material and the Darcy flow model, inertial effects must be considered. To test the XPHD lubrication mechanism beyond the limit of the Darcy model, the squeeze flow problem was described using the theoretical Darcy-Forchheimer model.

Since for the studied model there is no possible analytical solution, the problem is solved numerically by the finite difference method. The numerical model was used to evaluate the influence of various parameters of the extended model with the Forchheimer term. The obtained results show that the inertial effects have an important contribution to the force and pressure field generated during the compression of a porous material. The observation is particularly valid for high porosity materials imbibed with low viscosity fluids.

The numerical results obtained with the proposed flow model show an increase in pressure values through inertial effects, at the same level of compression of the porous structure. Therefore, the squeeze force is increased by inertial effects, a conclusion supported by the experimental results obtained by the Lubrication team that revealed compressions of imbibed porous materials lower than those theoretically predicted for impact (with Darcy model).

- With the help of an experimental device based on an original idea, it was possible to highlight the correlation between the level of compression, the compression force, and the volume of the fluid present in the porous layers. The experimental analysis is centered on the variation of porosity during constant-rate compression for easily deformable reticulated foams.

The remaining fluid volume, present even at very high deformations, shows the limit of the XPHD model, since the fluid flow in the material stops before reaching zero porosity, one of the basic assumptions of theoretical modeling. Upon reaching the critical porosity, the value of the occupied pore volume remains constant and independent of deformation. Critical porosity occurs near the upper limit of the densification zone.

- The experimental study of the influence of cyclic compression frequency on the behavior of some porous materials of interest shows that rewetting is an important condition when discussing this type of movement. The experimental results were obtained on an original device developed at Institute Pprime (Univ. of Poitiers).

The return stroke leads to the appearance of a negative pressure, closely related to the compression frequency. Its appearance was attributed to the phenomenon of re-absorption of fluid in the material, because of the development of a suction force between the compression plate and the material, which recovers the fluid squeezed during the compression stroke.

From the point of view of material influence, it is appreciated that the porosity, size, and shape of the pores influence the frequency up to which the material can continuously re-imbibe. The behavior of the material is also related to the fluid used, and it is necessary to choose a suitable material-fluid pair to highlight the beneficial effects of cyclic compression.

The maximum pressure increases linearly with the compression frequency up to values of 2 Hz for oil-imbibed materials and 5 Hz for water-imbibed ones. When the limiting frequency is reached, the reabsorption capacity of the material decreases, and the behavior becomes similar with the two fluids.

The cyclic compression process is influenced by the absorption, during the return stroke, of an increasingly important amount of air, which initially leads to the stagnation of the negative pressure and later the positive one. This result highlights the special attention that must be paid to the refilling conditions, so that the foam is permanently imbibed.

- Low-speed compression tests on S3DU material samples allow the evaluation of energy losses through hysteresis and highlight the appearance of a plastic component in the deformation mechanism of three-dimensional textile materials. The analysis of the morphological and mechanical characteristics of the material thus becomes an important activity to numerically simulate the behavior of the material under compression.

The reduction of the spacer structure to a representative periodic cell, using the scan of the material obtained on a computer tomograph, allowed to obtain simplified 3D models of the material in CAD programs. Starting from these, an advanced study of the compression behavior

of the material was carried out in a CAE environment, which allowed the extraction of the shapes of the distancing yarns at different levels of compression.

The deformed shapes were used to analyze in a CFD environment the flow of a fluid between the distancing yarns. The results of numerical simulations were compared with experimental data obtained for the same material, showing a very good level of correlation. The result of the comparison demonstrates the usefulness of numerical analysis methods in compressive permeability evaluation.

A second numerical study was performed to test the applicability limit of the Darcy flow model (on an undeformed cell) and compare the results with the extended theoretical model with the Darcy-Forchheimer correction. The numerical results obtained, for two fluids used in the CFD analysis, show that the permeability of the material does not depend on the fluid (as long as the temperature remains constant). This is a major advantage of using numerical methods to determine the permeability of a porous material, in contrast to experimental results where an influence of the fluid on the measured permeability values is frequently observed, caused by microscopic or macroscopic reactions between the fluid and the material.

It is also observed that for the analyzed flow domain ($Re_\phi < 23$), the Darcy-Forchheimer model provides a sufficiently good degree of approximation. Data processing shows a slight variation of permeability with flow regime, consistent with observations found in the literature. However, the question arises whether the method of interpretation of the experimental or numerical data, depending on the flow regime, does not actually lead to misinterpretations of the results, especially when a unitary approach is not identified in the literature on how to determine the Reynolds number specific to porous materials.

Considering all the simplifications made to obtain the deformation behavior of the distancing yarns and the permeability of the distancing layer, through numerical simulations performed in CAE and CFD environments, the results obtained are excellent. Of course, the whole process can be improved, optimized, or reanalyzed at certain points, starting from the CT scan and ending with the numerical model.

The results represent a good starting point for future approaches in this field and the models made can be used to design materials adapted to the damping needs of an application.

6.2 PERSONAL CONTRIBUTIONS

The studies carried out within the doctoral program contribute to the analysis of the flow of liquids through highly deformable porous media subjected to compression. Two categories of relatively new porous media were targeted for use: fibrous materials from the category of three-dimensional textiles (Spacer 3D), respectively reticulated foams with communicating pores.

- Mathematical model and related numerical code, developed in FORTRAN language, for the simulation of planar, axisymmetric flow of a Newtonian liquid through a porous, deformable structure subject to compression.
- Highlighting the influence of the velocity flow through the pores of the material (the effect of the Forchheimer inertial term) on the pressure field generated by planar radial squeeze of a Newtonian liquid.

- Device for determining the critical porosity (practical limit of permeability) and its correlation with the characteristic compression curve of the porous structure.
- Conceptual design of the mechanism for converting rotational motion into reciprocating translation, for the cyclic compression bench.
- Highlighting the limiting frequency up to which imbibed porous materials, subjected to cyclic compression, have damping capacity and its correlation with reabsorption capacity.
- Generation of a solid model (representative cell) of the structure of a Spacer 3D textile material starting from the micro-tomographic scan.
- Numerical simulation of non-linear compressive structural behavior of Spacer 3D material and correlation with experimental data.
- Complex numerical simulation in ANSYS-Fluent of the flow of a Newtonian fluid through the compressed 3D structure for the purpose of determining bidirectional in-plane permeability.
- Highlighting the limitation of using the Darcy model for permeability calculation.
- Determination of the permeability-porosity correlation at different levels of compression and comparison with previously obtained experimental results.

6.3 FUTURE RESEARCH DIRECTIONS

The obtained results lead to the definition of the following directions of evolution:

- Experimental verification of the data obtained from solving the numerical model, for the simulation of planar, axially symmetric flow of a Newtonian liquid through a porous, deformable structure subjected to compression.
- Extending the mathematical model and numerical code by using the axial component of the squeezed fluid flow velocity.
- Extending the mathematical model and calculation program by using more complex theoretical flow models and or with other types of loads, such as constant force or impact with given impulse, and validating them with experimental data.
- Development of an improved version of the critical porosity tester for testing a wider range of materials.
- Modification of the cyclic compression bench test cell to improve refilling conditions at higher frequencies by expanding the tank capacity or using a closed test cell.
- Characterization of several porous material-fluid pairs subjected to cyclic compression to identify an optimal variant for the XPHD mechanism.
- Numerical modeling of the behavior of imbibed porous materials subjected to cyclic stresses.
- Numerical study of the permeability by means of CFD considering the influence of the porosity of the layers of a three-dimensional textile material and the determination of both in-plane permeabilities and the one corresponding to transverse flow.
- Numerical study of the permeability by means of CFD and statistical analysis of the tortuosity of the flow lines through the distancing yarns.
- Use of other flow models for numerical evaluation of permeability and comparison with results obtained with the laminar flow model.

SELECTIVE BIBLIOGRAPHY

[1] ***, https://www.dimer.com/en/materialien/pur-weichschaum/pur-schaum.php

[2] ***, *PROTHEIS - Sisteme de protecție împotriva impacturilor de energie mare și a exploziilor folosind materiale poroase îmbibate cu lichide*, PN-II-Nr.287/2014, grant 2014-2017, Universitatea Politehnica din București

[3] ***, https://www.heathcoat.co.uk/

[4] Antohe B. V., Lage J. L., Price D. C., Weber R. M., 1997, *Experimental determination of permeability and inertia coefficients of mechanically compressed aluminum porous matrices*, Journal of Fluids Engineering, vol. 119, nr. 2, p. 404–412

[5] Bardenhagen S. G., Brydon A. D., Guilkey J. E., 2005, *Insight into the physics of foam densification via numerical simulation*, Journal of the Mechanics and Physics of Solids, vol. 53, nr. 3, p. 597–617

[6] Bear J., 1972, *Dynamics of fluids in porous media*, Ed. Elsevier, New York

[7] Bear J., 2018, *Modeling phenomena of flow and transport in porous media*, ed. 1, Ed. Springer International Publishing, Cham

[8] Bear J., Zaslavsky D., Irmay S., 1968, *Physical principles of water percolation and seepage*, UNESCO, Paris

[9] Beavers G. S., Sparrow E. M., Rodenz D. E., 1973, *Influence of Bed Size on the Flow Characteristics and Porosity of Randomly Packed Beds of Spheres*, Journal of Applied Mechanics, vol. 40, nr. 3, p. 655–660

[10] Boomsma K., Poulikakos D., 2002, *The effects of compression and pore size variations on the liquid flow characteristics in metal foams*, Journal of Fluids Engineering, vol. 124, nr. 1, p. 263–272

[11] Bowden F., Tabor D., 1950, *The friction and lubrication of solids*, Ed. Clarendon Press, Oxford, pp. 259-284

[12] Brinkman H. C., 1949, *A calculation of the viscous force exerted by a flowing fluid on a dense swarm of particles*, Flow, Turbulence and Combustion, vol. 1, nr. 1, p. 27–34

[13] Carman P. C., 1937, *Fluid flow through granular beds*, Transactions of the Institution of Chemical Engineers (London), vol. 15, p. 150–166

[14] Chapman R. E., 1981, *Geology and Water*, Ed. Martinus Nijhoff/Dr W. Junk Publishers bv, The Hague

[15] Cicone T., Pascovici M. D., Melciu C., Turtoi P., 2019, *Optimal porosity for impact squeeze of soft layers imbibed with liquids*, Tribology International, vol. 138, p. 140–149

[16] Couderc B., Lupu G. C., Henry Y., Fatu A., Bouyer J., 2023, *Characterization of soaked soft porous materials under cyclic compression (Caractérisation de matériaux poreux imbibés sous compression cyclique)* in 22nd Pprime Workshop: How can hydrodynamic bearings be used in low-speed applications?, Poitiers

[17] Darcy H. P. G., 1856, *Les Fontaines Publiques de la Ville de Dijon*, Ed. Victor Dalmont, Paris

[18] Dawson M. A., 2008, *Modeling the dynamic response of low-density, reticulated, elastomeric foam impregnated with Newtonian and non-Newtonian fluids*, Teză de doctorat, MIT

[19] Dawson M. A., 2009, *Composite plates with a layer of fluid-filled, reticulated foam for blast protection of infrastructure*, International Journal of Impact Engineering, vol. 36, nr. 10–11, p. 1288–1295

[20] Dawson M. A., Germaine J. T., Gibson L. J., 2007, *Permeability of open-cell foams under compressive strain*, International Journal of Solids and Structures, vol. 44, nr. 16, p. 5133–5145

[21] Dawson M. A., McKinley G. H., Gibson L. J., 2008, *The dynamic compressive response of open-cell foam impregnated with a newtonian fluid*, Journal of Applied Mechanics, vol. 75, nr. 4, p. 041015

[22] Dawson M. A., McKinley G. H., Gibson L. J., 2009, *The dynamic compressive response of an open-cell foam impregnated with a non-newtonian fluid*, Journal of Applied Mechanics, vol. 76, nr. 6, p. 061011

[23] Dupuit A. J. É., 1863, *Études théoriques et pratiques sur le mouvement des eaux dans les canaux découverts et à travers les terrains perméables*, ed. 2, Ed. Librairie des corps impérial des ponts et chaussées et des mines, Paris

[24] Dybbs A., Edwards R. V., 1984, *A new look at porous media fluid mechanics — Darcy to turbulent* in Fundamentals of Transport Phenomena in Porous Media, Ed. Springer Netherlands, Dordrecht, p. 199–256

[25] Emersleben O., 1925, *Das Darcysche filtergesetz*, Physikalische Zeitschrift, vol. 26, p. 601–610

[26] Enescu C., Turtoi P., Cicone T., Istrate C. V., 2020, *Experimental assessment of permeability variation with the compression of soft reticulated foams*, IOP Conference Series: Materials Science and Engineering, vol. 997, nr. 1, p. 012009

[27] Enescu C., Turtoi P., Stanciu M., Cicone T., 2021, *Preliminary experimental assessment of radial flow permeability variation with the compression level of 3D fabrics*, The 9th International Conference on Computational Mechanics and Virtual Engineering (COMEC 2021), Brasov, ROMANIA

[28] Feng J., Weinbaum S., 2000, *Lubrication theory in highly compressible porous media: the mechanics of skiing, from red cells to humans*, Journal of Fluid Mechanics, vol. 422, p. 281–317

[29] Forchheimer P., 1901, *Wasserberwegung durch Boden*, Zeitschrift Des Vereines Deutscher Ingenieure, vol. 45, p. 1782–1788

[30] Fourar M., Radilla G., Lenormand R., Moyne C., 2004, *On the non-linear behavior of a laminar single-phase flow through two and three-dimensional porous media*, Advances in Water Resources, vol. 27, nr. 6, p. 669–677

[31] Gartling D. K., Hickox C. E., Givler R. C., 1996, *Simulation of Coupled Viscous and Porous Flow Problems*, International Journal of Computational Fluid Dynamics, vol. 7, nr. 1–2, p. 23–48

[32] Gebart B. R., 1992, *Permeability of Unidirectional Reinforcements for RTM*, Journal of Composite Materials, vol. 26, nr. 8, p. 1100–1133

[33] Gent A. N., Rusch K. C., 1966, *Permeability of open-cell foamed materials*, Journal of Cellular Plastics, vol. 2, nr. 1, p. 46–51

[34] Ghaddar C. K., 1995, *On the permeability of unidirectional fibrous media: A parallel computational approach*, Physics of Fluids, vol. 7, nr. 11, p. 2563–2586

[35] Gibson L. J., Ashby M. F., 1999, *Cellular solids. Structure and properties*, Ed. Cambridge University Press,

[36] Gioia G., Wang Y., Cuitiño A. M., 2001, *The energetics of heterogeneous deformation in open-cell solid foams*, Proceedings of the Royal Society of London. Series A: Mathematical, Physical and Engineering Sciences, vol. 457, nr. 2009, p. 1079–1096

[37] Gutowski T. G., Cai Z., Bauer S., Boucher D., Kingery J., Wineman S., 1987, *Consolidation experiments for laminate composites*, Journal of Composite Materials, vol. 21, nr. 7, p. 650–669

[38] Gutowski T. G., Morigaki T., Zhong Cai, 1987, *The consolidation of laminate composites*, Journal of Composite Materials, vol. 21, nr. 2, p. 172–188

[39] Happel J., Brenner H., 1981, *Low Reynolds number hydrodynamics: with special applications to particulate media*, Ed. Martinus Nijhoff Publishers, The Hague

[40] Hou X., Hu H., Liu Y., Silberschmidt V., 2011, *Nonlinear compression behavior of warp-knitted spacer fabric: effect of sandwich structure*, Computers, Materials and Continua, vol. 23, nr. 2, p. 119–134

[41] Ilie M.-B., 2011, *Capacitatea de amortizare a straturilor poroase, foarte compresibile, îmbibate cu lichide, pentru configurații cilindrice*, Teză de doctorat, Facultatea de Inginerie Mecanică și Mecatronică, Universitatea Politehnica din București

[42] Ilie M.-B., Cicone T., Pascovici M., 2012, *Accuracy of analytical models for squeeze of rigid spheres on highly compressible porous layers imbibed with liquids*, Journal of the Balkan Tribological Association, vol. 18, p. 124–132

[43] Ilie M.-B., Pascovici M., Cicone T., Predescu A., 2011, *Compliant porous layers imbibed with liquids squeezed at constant velocity by a rigid sphere*, PUB Scientific Bulletin, Series D: Mechanical Engineering, vol. 73, p. 111–124

[44] Ilie M.-B., Pascovici M. D., Marian V. G., 2011, *Squeeze processes in a narrow circular damper with highly compressible porous layer imbibed with liquids*, Proceedings of the Institution of Mechanical Engineers, Part J: Journal of Engineering Tribology, vol. 225, nr. 6, p. 539–549

[45] Jackson G. W., James D. F., 1986, *The permeability of fibrous porous media*, The Canadian Journal of Chemical Engineering, vol. 64, nr. 3, p. 364–374
[46] Joseph D. D., Nield D. A., Papanicolaou G., 1982, *Nonlinear equation governing flow in a saturated porous medium*, Water Resources Research, vol. 18, nr. 4, p. 1049–1052
[47] Joseph D. D., Nield D. A., Papanicolaou G., 1983, *Correction to 'Nonlinear equation governing flow in a saturated porous medium' by D. D. Joseph et al.*, Water Resources Research, vol. 19, nr. 2, p. 591–591
[48] Kozeny J., 1927, *Uber kapillare Leitung des Wassers im Boden* in Stizungsber Royal Academy of Science, Proceedings Class I, Viena, p. 271–306
[49] Kunik S., 2018, *Étude numérique et expérimentale du mécanisme de lubrification Ex-Poro-HydroDynamique (XPHD)*, Teză de doctorat, Université de Poitiers
[50] Lage J. L., Antohe B. V., 2000, *Darcy's experiments and the deviation to nonlinear flow regime*, Journal of Fluids Engineering, vol. 122, nr. 3, p. 619–625
[51] Lage J. L., Antohe B. V., Nield D. A., 1997, *Two types of nonlinear pressure-drop versus flow-rate relation observed for saturated porous media*, Journal of Fluids Engineering, vol. 119, nr. 3, p. 700–706
[52] Lage J. L., De Lemos M. J. S., Nield D. A., 2002, *Modeling turbulence in porous media* in Transport phenomena in porous media II, Ed. Elsevier,, p. 198–230
[53] Li Q. M., Mines R. A. W., Birch R. S., 2000, *The crush behaviour of Rohacell-51WF structural foam*, International Journal of Solids and Structures, vol. 37, nr. 43, p. 6321–6341
[54] Liu Y., Hu H., Zhao L., Long H., 2012, *Compression behavior of warp-knitted spacer fabrics for cushioning applications*, Textile Research Journal, vol. 82, nr. 1, p. 11–20
[55] Lundström T. S., Stenberg R., Bergström R., Partanen H., Birkeland P. A., 2000, *In-plane permeability measurements: a nordic round-robin study*, Composites Part A: Applied Science and Manufacturing, vol. 31, nr. 1, p. 29–43
[56] Lupu G. C., Fatu A., Henry Y., Nechita I. R., Cicone T., 2023, *Experimental investigation of imbibed open-cell foams under repetitive compression*, Acceptat Pentru Publicare În PUB Scientific Bulletin, Series D: Mechanical Engineering
[57] Lupu G. C., Fătu A., Henry Y., Turtoi P., Cicone T., 2022, *Mechanical and structural characterisation of a 3D warp-knitted spacer fabric subjected to compression*, IOP Conference Series: Materials Science and Engineering, vol. 1262, nr. 1, p. 012024
[58] Lupu G., Turtoi P., Cicone T., 2020, *Evaluation of inertia effects in planar squeeze flow inside soft, porous layers*, IOP Conference Series: Materials Science and Engineering, vol. 724, nr. 1, p. 012042
[59] May D., Aktas A., Advani S. G., Berg D. C., Endruweit A., Fauster E., et al., 2019, *In-plane permeability characterization of engineering textiles based on radial flow experiments: A benchmark exercise*, Composites Part A: Applied Science and Manufacturing, vol. 121, p. 100–114
[60] Melciu I. C., 2020, *Procese de expulzare repetative în medii complexe*, Teză de doctorat, Facultatea de Inginerie Mecanică și Mecatronică, Universitatea Politehnica din București
[61] Melciu I. C., Cicone T., Pascovici M. D., 2017, *Saturated porous layers squeezed between parallel disks in enclosed cells*, IOP Conference Series: Materials Science and Engineering, vol. 174, p. 012031
[62] Melciu I. C., Pascovici M. D., 2018, *The squeeze of an imbibed soft porous media in contact with a plastic body at impact loading. A heuristic model*, U.P.B. Scientific Bulletin, Series D, vol. 80, nr. 4, p. 205–222
[63] Miltz J., Gruenbaum G., 1981, *Evaluation of cushioning properties of plastic foams from compressive measurements*, Polymer Engineering and Science, vol. 21, nr. 15, p. 1010–1014
[64] Mirbod P., Andreopoulos Y., Weinbaum S., 2009, *On the generation of lift forces in random soft porous media*, Journal of Fluid Mechanics, vol. 619, p. 147–166
[65] Nabhani M., El Khlifi M., Bou-Saïd B., 2009, *Etude de l'écrasement d'un film sur un milieu poreux modélisé par l'équation de Darcy-Forchheimer* in 9ème Congrès International de Mécanique, Marrakech, p. 10–12
[66] Nabhani M., El Khlifi M., Bou-saïd B., 2010, *A numerical simulation of viscous shear effects on porous squeeze-film using the Darcy-Brinkman model*, Mécanique & Industries, vol. 11, nr. 5, p. 327–337

[67] Nabhani M., El Khlifi M., Bou-Saïd B., 2010, *A general model for porous medium flow in squeezing film situations*, Lubrication Science, vol. 22, nr. 2, p. 37–52
[68] Nield D. A., Bejan A., 2006, *Convection in porous media*, ed. 3, Ed. Springer, New York
[69] Orlik J., Pietsch K., Fassbender A., Sivak O., Steiner K., 2018, *Simulation and experimental validation of spacer fabrics based on their structure and yarn's properties*, Applied Composite Materials, vol. 25, nr. 4, p. 709–724
[70] Panfilov M., Fourar M., 2006, *Physical splitting of nonlinear effects in high-velocity stable flow through porous media*, Advances in Water Resources, vol. 29, nr. 1, p. 30–41
[71] Papathanasiou T. D., Markicevic B., Dendy E. D., 2001, *A computational evaluation of the Ergun and Forchheimer equations for fibrous porous media*, Physics of Fluids, vol. 13, nr. 10, p. 2795–2804
[72] Pascovici M. D., 1994, *Procedure and device for pumping by fluid dislocation, patent nr. 109469*,
[73] Pascovici M. D., 2001, *Lubrication by dislocation: a new mechanism for load carrying capacity* in Proceedings of 2nd World Tribology Congress, vol. 41, Vienna
[74] Pascovici M. D., 2007, *Lubrication processes in highly compressible porous layers* in Lubrification et tribologie des revêtements minces, Ed. Presses polytechniques et universitaires romandes, Poitiers, p. 3–12
[75] Pascovici M. D., 2007, *Lubrication of red blood cells in narrow capillaries. A heuristic approach* in 2nd Vienna International Conference on Micro and Nanotechnology, p. 95-100
[76] Pascovici M. D., Cicone T., 2003, *Squeeze-film of unconformal, compliant and layered contacts*, Tribology International, vol. 36, nr. 11, p. 791–799
[77] Pascovici M. D., Popescu C. S., Marian V. G., 2010, *Impact of a rigid sphere on a highly compressible porous layer imbibed with a Newtonian liquid*, Proceedings of the Institution of Mechanical Engineers, Part J: Journal of Engineering Tribology, vol. 224, nr. 8, p. 789–795
[78] Pascovici M., Russu C., Cicone T., 2004, *Squeeze film of conformal, layered, compliant and porous contacts*, The 9th International Conference of Mechanisms and Mechanical Transmissions, Acta Tehnica Napocensis, Applied Mathematics and Mechanics, vol. 47, nr. I
[79] Popescu C. S., 2010, *Procese de curgere în straturi poroase, foarte compresibile, supuse la sarcini de impact*, Teză de doctorat, Facultatea de Inginerie Mecanică și Mecatronică, Universitatea Politehnica din București
[80] Popescu C. S., 2011, *Numerical study of dynamic loading in ex-porohydrodynamic lubrication. 3D case study: Human footprint impact over a highly compressible porous layer saturated with water*, PUB Scientific Bulletin, Series D: Mechanical Engineering, vol. 73, nr. 2, p. 279–290
[81] Radu M., 2015, *Modelarea și simularea procesului de expulzare al fluidelor prin straturi poroase extrem de compresibile prin impact*, Teză de doctorat, Facultatea de Inginerie Mecanică și Mecatronică, Universitatea Politehnica din București
[82] Radu M., Cicone T., 2016, *Experimental determination of the damping capacity of highly compressible porous materials imbibed with water*, Journal of the Balkan Tribological Association, vol. 22, nr. 1, p. 390–400
[83] Raeini A. Q., Blunt M. J., Bijeljic B., 2014, *Direct simulations of two-phase flow on micro-CT images of porous media and upscaling of pore-scale forces*, Advances in Water Resources, vol. 74, p. 116–126
[84] Rodrigues A., Figueiredo L., Diogo H., Bordado J., 2018, *Mechanical behavior of PET fibers and textiles for Stent-Grafts using video extensometry and image analysis*, Science and Technology of Materials, vol. 30, p. 23–33
[85] Rouquerol J., Avnir D., Fairbridge C. W., Everett D. H., Haynes J. M., Pernicone N., Ramsay J. D. F., Sing K. S. W., Unger K. K., 1994, *Recommendations for the characterization of porous solids (Technical Report)*, Pure and Applied Chemistry, vol. 66, nr. 8, p. 1739–1758
[86] Roye A., Stuve J., Gries T., 2005, *Definition for the differentiation of 2D- and 3D- textiles – part 1: Production in one-step-processes*, Narrow Fabric and Braiding Industry, vol. 124, nr. 2, p. 46–49
[87] Russu C., 2008, *Contribuții la reologia și poro-hidrodinamica lubrificației*, Teză de doctorat, Facultatea de Inginerie Mecanică și Mecatronică, Universitatea Politehnica din București
[88] Scheidegger A. E., 1974, *The physics of flow through porous media*, Ed. University of Toronto Press, Toronto
[89] Stock S. R., 2008, *Recent advances in X-ray microtomography applied to materials*, International Materials Reviews, vol. 53, nr. 3, p. 129–181

[90] Tek M., 1957, *Development of a generalized Darcy equation*, Journal of Petroleum Technology, vol. 9, nr. 06, p. 45–47
[91] Truskey G. A., Yuan F., Katz D. F., 2004, *Transport phenomena in biological systems*, ed. 2, Ed. Pearson Prentice Hall, Upper Saddle River (New Jersey)
[92] Turtoi P., 2016, *Contribuții la studiul proceselor de expulzare prin medii complexe*, Teză de doctorat, Facultatea de Inginerie Mecanică și Mecatronică, Universitatea Politehnica din București
[93] Turtoi P., Cicone T., Fatu A., 2017, *Experimental and theoretical analysis of (water) permeability variation of nonwoven textiles subjected to compression*, Mechanics & Industry, vol. 18, nr. 3, p. 307
[94] Turtoi P., Lupu G., Cicone T., Apostol D., 2020, *Experimental investigation of the limits of fluid squeeze out from an imbibed porous material*, IOP Conference Series: Materials Science and Engineering, vol. 997, nr. 1, p. 012019
[95] Turtoi P., Pascovici M. D., 2016, *Finite volume squeeze flow in highly compressible porous annular discs*, U.P.B. Scientific Bulletin, Series D, vol. 78, nr. 2, p. 43–56
[96] Turtoi P., Pascovici M. D., Cicone T., Rotariu A. N., Puică C. C., Istrate M., 2018, *Experimental proof of squeeze damping capacity of imbibed soft porous layers subjected to impact*, IOP Conference Series: Materials Science and Engineering, vol. 444, p. 022010
[97] Turtoi, Pascovici, Cicone, 2019, *Squeeze Flow of Bingham Fluids through Reticulated, Compressed Foams*, Lubricants, vol. 7, nr. 10, p. 86
[98] Vossen B., 2010, *Modelling the application of fluid filled foam in motorcycle helmets*, Raport de cercetare, Eindhoven University of Technology și MIT, Eindhoven
[99] de Vries J., 1979, *Prediction of non-Darcy flow in porous media*, Journal of the Irrigation and Drainage Division, vol. 105, nr. 2, p. 147–162
[100] Wang L., Li Y., Zhao G., Chen N., Xu Y., 2019, *Experimental investigation of flow characteristics in porous media at low Reynolds numbers (Re→0) under different constant hydraulic heads*, Water, vol. 11, nr. 11, p. 2317
[101] Wang X. H., Kainuma M., Bao L. M., Nakazawa M., 2006, *A novel approach for evaluating the air permeability of airbag fabrics*, Textile Research Journal, vol. 76, nr. 1, p. 66–70
[102] Ward J. C., 1964, *Turbulent flow in porous media*, Journal of the Hydraulics Division, vol. 90, nr. 5, p. 1–12
[103] Wu Q., Andreopoulos Y., Weinbaum S., 2004, *From Red Cells to Snowboarding: A New Concept for a Train Track*, Physical Review Letters, vol. 93, nr. 19, p. 194501
[104] Wu Q., Andreopoulos Y., Xanthos S., Weinbaum S., 2005, *Dynamic compression of highly compressible porous media with application to snow compaction*, Journal of Fluid Mechanics, vol. 542, p. 281–304
[105] Ye X., Fangueiro R., Hu H., Araújo M. de, 2007, *Application of warp-knitted spacer fabrics in car seats*, Journal of the Textile Institute, vol. 98, nr. 4, p. 337–344
[106] Ye X., Hu H., Feng X., 2008, *Development of the warp knitted spacer fabrics for cushion applications*, Journal of Industrial Textiles, vol. 37, nr. 3, p. 213–223

DISSEMINATION OF RESULTS

SCIENTIFIC RESEARCH REPORTS

Lupu, GC, July 2019, *Squeeze processes in highly compressible porous media. Mathematical models*, Scientific Research Report no. 1, Doctoral School of Mechanical and Mechatronic Engineering, Polytechnic University of Bucharest

Lupu, GC, July 2020, *Analysis of the applicability limits of the XPHD lubrication model in the case of reticulated foams*, Scientific Research Report no. 2, Doctoral School of Mechanical and Mechatronic Engineering, Polytechnic University of Bucharest

Lupu, GC, May 2022, *Morphological and mechanical characterization of three-dimensional textile materials*, Scientific research report no. 3, Doctoral School of Mechanical and Mechatronic Engineering, Polytechnic University of Bucharest

Lupu, GC, May 2022, *Experimental study of the periodic compression behavior of soaked porous materials*, Scientific research report no. 4, Doctoral School of Mechanical and Mechatronic Engineering, Polytechnic University of Bucharest

SCIENTIFIC PAPERS PUBLISHED OR UNDER PUBLICATION

(1) **Lupu G.**, Turtoi P., Cicone T., 2020, - *Evaluation of inertia effects in planar squeeze flow inside soft, porous layers*, IOP Conference Series: Materials Science and Engineering, vol. 724 (1), p. 012042, doi: 10.1088/1757-899X/724/1/012042 (**WOS000619349400042**)

(2) Turtoi P., **Lupu G.**, Cicone T., Apostol D., 2020, *Experimental investigation of the limits of fluid squeeze out from an imbibed porous material*, IOP Conference Series: Materials Science and Engineering, vol. 997 (1), p 012019, doi:10.1088/1757-899X/997/1/012019 (**SCOPUS**)

(3) **Lupu GC**, Fătu A., Henry Y., Turtoi P., Cicone T., 2022, *Mechanical and structural characterization of a 3D warp-knitted spacer fabric subjected to compression*, IOP Conference Series: Materials Science and Engineering, vol. 1262 (1), p. 012024, doi:10.1088/1757-899X/1262/1/012024, (IOP Publishing - **BDI**)

(4) **Lupu GC**, Fătu A., Henry Y., Nechita RI, Cicone T., 2023, *Experimental investigation of imbibed open-cell foams under repetitive compression* accepted for publication (15.09.2023) in PUB Scientific Bulletin. Series D: Mechanical Engineering (**SCOPUS)**

(5) Couderc B., **Lupu GC,** Henry Y., Fătu A., Bouyer J., 2023, *Characterization of soaked soft, porous materials under cyclic compression* – to be submitted for publication in Mécanique & Industries journal

PRESENTATIONS AT INTERNATIONAL SCIENTIFIC EXHIBITIONS

(1) **Lupu G.**, Turtoi P., Cicone T., 2020, *Evaluation of inertia effects in planar squeeze flow inside soft, porous layers* Proceedings of the 14th International Conference on Tribology, ROTRIB'19, 19-21 September 2019, Cluj-Napoca, Romania

(2) Turtoi P., **Lupu G.**, Cicone T., Apostol D., 2020, *Experimental investigation of the limits of fluid squeeze out from an imbibed porous material*, Proceedings of the 9th International Conference on Advanced Concepts in Mechanical Engineering (ACME 2020), June 4-5, 2020, Iasi, Romania

(3) **Lupu GC**, Fătu A., Henry Y., Turtoi P., Cicone T., 2022, *Mechanical and structural characterization of a 3D warp-knitted spacer fabric subjected to compression*, Proceedings of the 10th International Conference on Advanced Concepts in Mechanical Engineering (ACME 2022), June 9-10, 2022, Iasi, Romania

(4) Couderc B., **Lupu GC**, Henry Y., Fătu A., Bouyer J., 2023, *Characterization of soaked soft, porous materials under cyclic compression* - 22nd Tribo–Pprime workshop " *How can hydrodynamic bearings be used in low-speed applications?* ", 12-13 October 2023, Poitiers, France